Applications of TEM imaging, analysis and electron holography to III-nitride HEMT devices

David J. Smith, David A. Cullen, Michael Johnson, Lin Zhou and Martha R. McCartney

Department of Physics
Arizona State University

Work supported by AFRL Contract FA-8650-08-C-1595 (Monitor: C. Bozada) and Wyle Laboratory Contract #DD-8192 (Monitor: S. Tetlak).

TiAlNiAu contacts for ultrathin AlN/GaN HEMT

Work in collaboration with C. Chang, F. Ren, and S. Pearton (U Florida)

Effect of annealing temperature

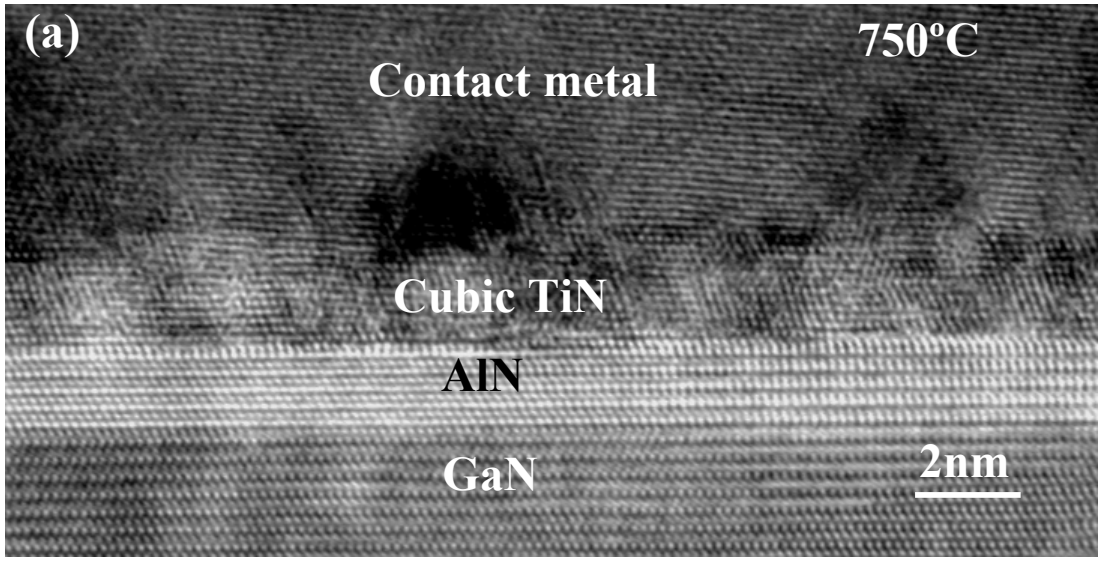

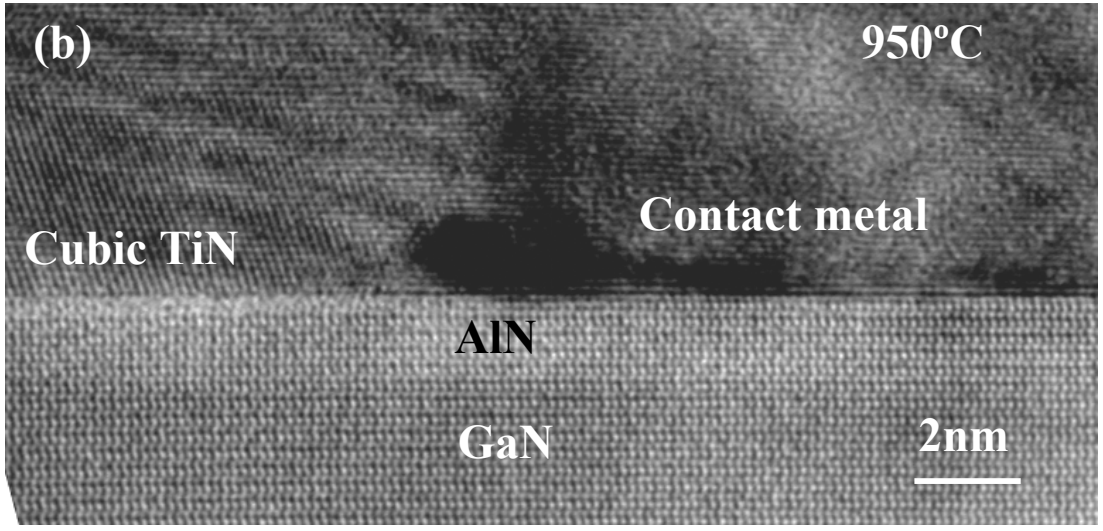

HREM TEM images of AlN/GaN HEMT structure.

- Cubic TiN changes from continuous layer into isolated islands with increasing annealing temperature.

Contact inclusions: morphology

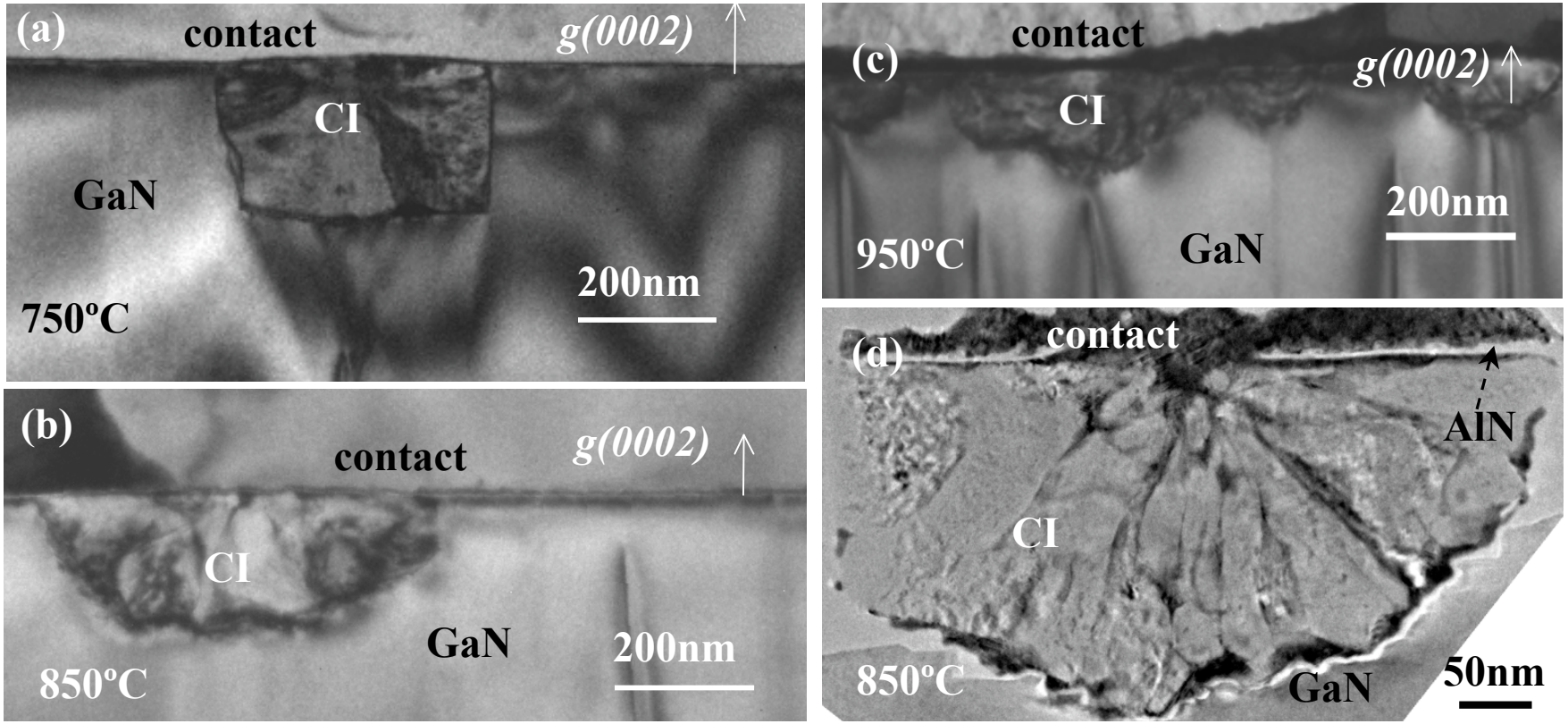

Two-beam diffraction contrast XTEM images showing contact inclusions.

- The contact inclusions penetrate beyond AlN/GaN interface into GaN layer along threading dislocations.

Contact inclusions: effect of annealing temperature

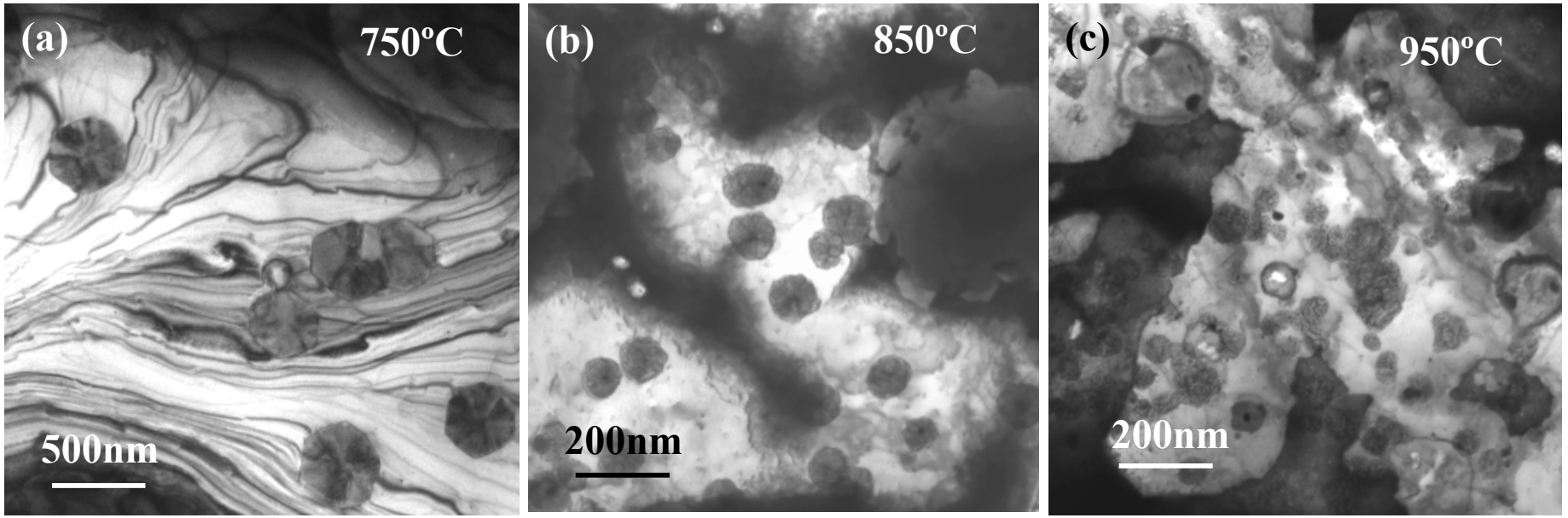

Plan-view TEM images of AlN/GaN HEMT.

- Density of hexagonal-shaped CIs increases with annealing temperature.

Contact inclusions and contact resistance

Sample	*AT (°C)*	*CI density* (cm^{-2})	$t_{GaN\ capping}$ (*nm*)	t_{AlN} (*nm*)	*SR ** (*ohm/sq*)	*CR** ($ohm \cdot cm^2$)
A	No contact	0	~1	~2.5		
B	No annealing	0	~1	~2.5		
C	750	~5×10^7	0	~2.5	917	2.9e-5
D	850	~1×10^9	0	~2.5	479	1.5e-5
E	950	~7×10^9	0	~2.5	2.5E9	90.4

SR: sheet resistance; CR: specific contact resistivity

- Contact resistivity increased with increased CI density after 850ºC annealing.

Zhou *et. al.*, JAP., 108 (2010) 084513

Ohmic contacts for AlInN HFETs

Work in collaboration with J.Leach, H. Morkoç (VCU)

Contact (Au/Ni/Al/Ti) vs. annealing temperature

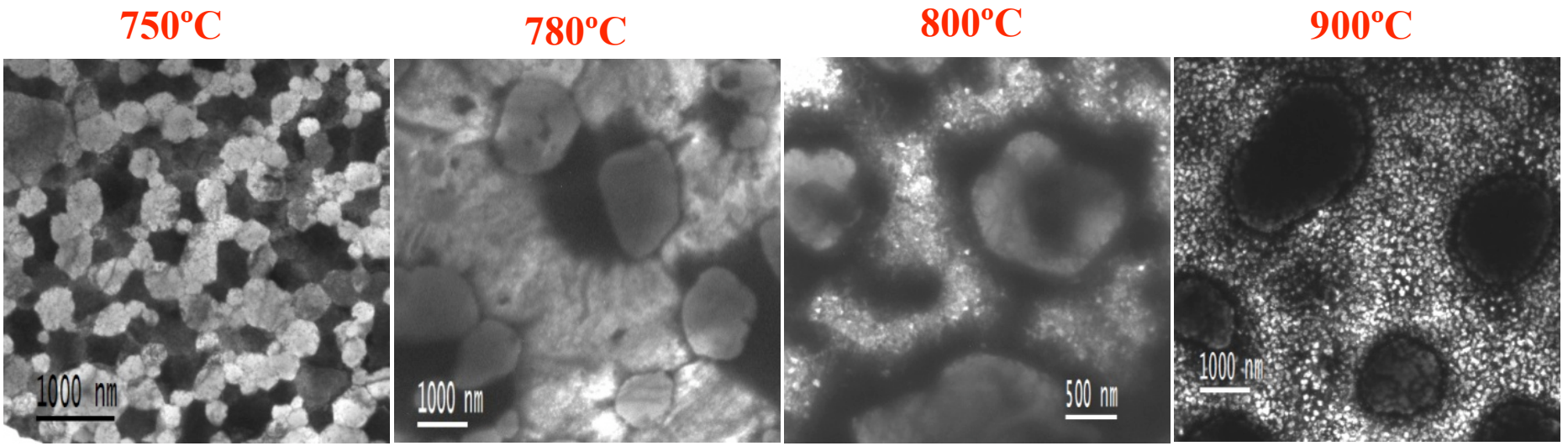

Plan-view TEM images showing changing morphology of Ti/Al/Ni/Au contacts.

- Intermixing of different metal layers.
- Morphology changed dramatically in sample annealed at 780ºC.
- Distinctive network structure in sample annealed at 900ºC.

Effect of annealing temperature

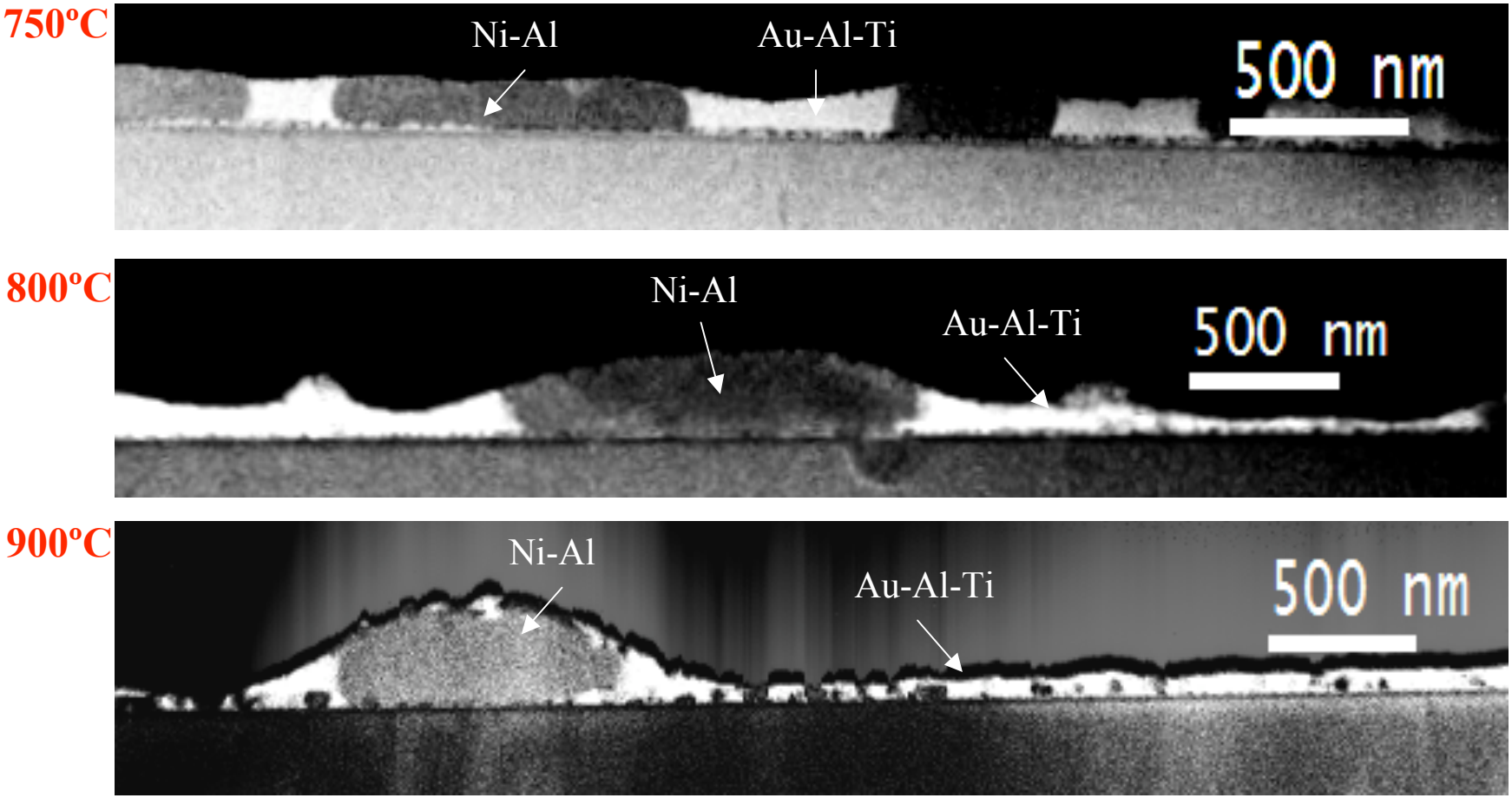

Cross-sectional HAADF STEM images.

- Contact surface bulged up with increasing temperature due to formation of ellipsoidal Ni-Al intermetallic particles embedded in Al-Au matrix.

Effect of annealing temperature

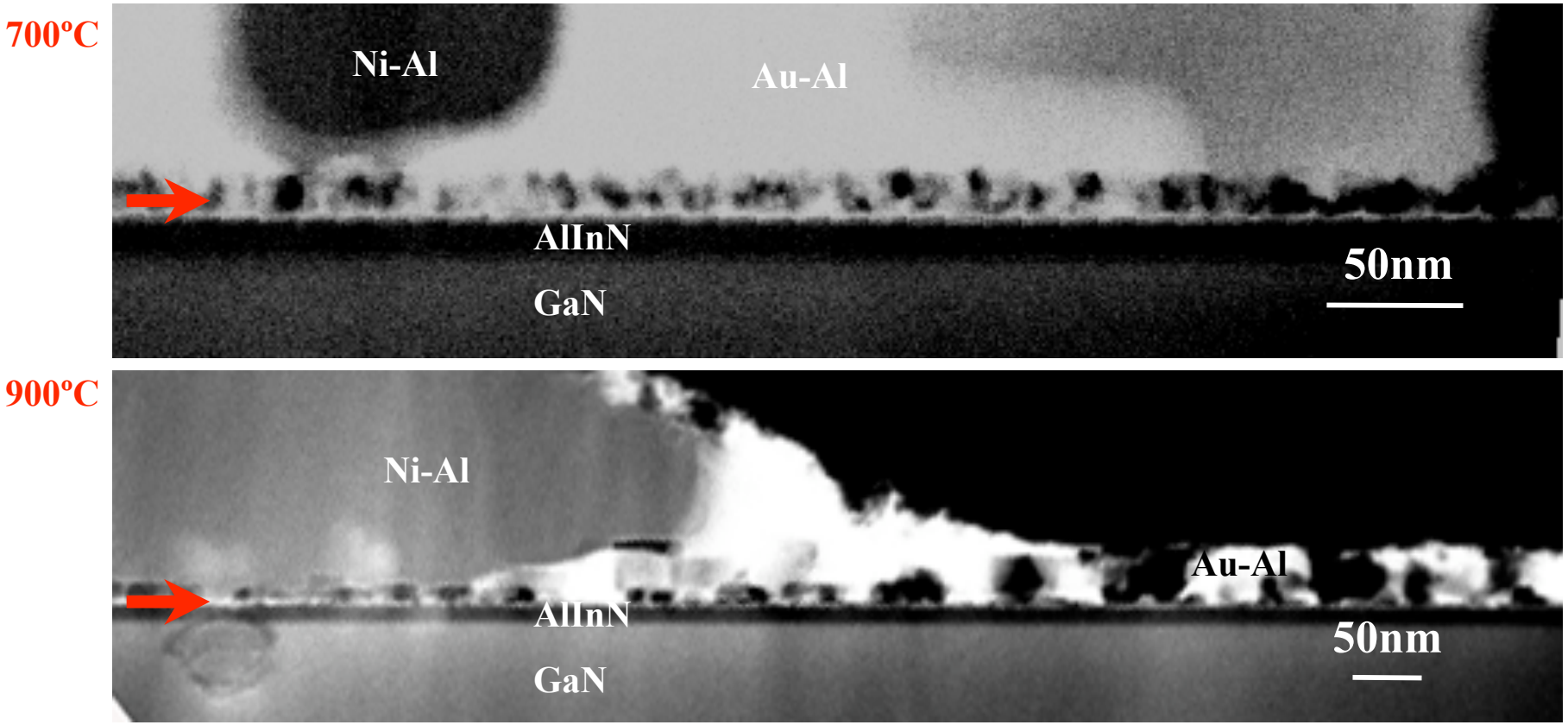

Cross-sectional HAADF STEM images.

- ~25-nm-thick porous Ti-rich layer (arrowed) below Ni-Al and Au-Al alloys for samples annealed below 850ºC.
- Porous Ti-rich layer (arrowed) only observed underneath Ni-Al particles for samples annealed above 850ºC.

Contact inclusions

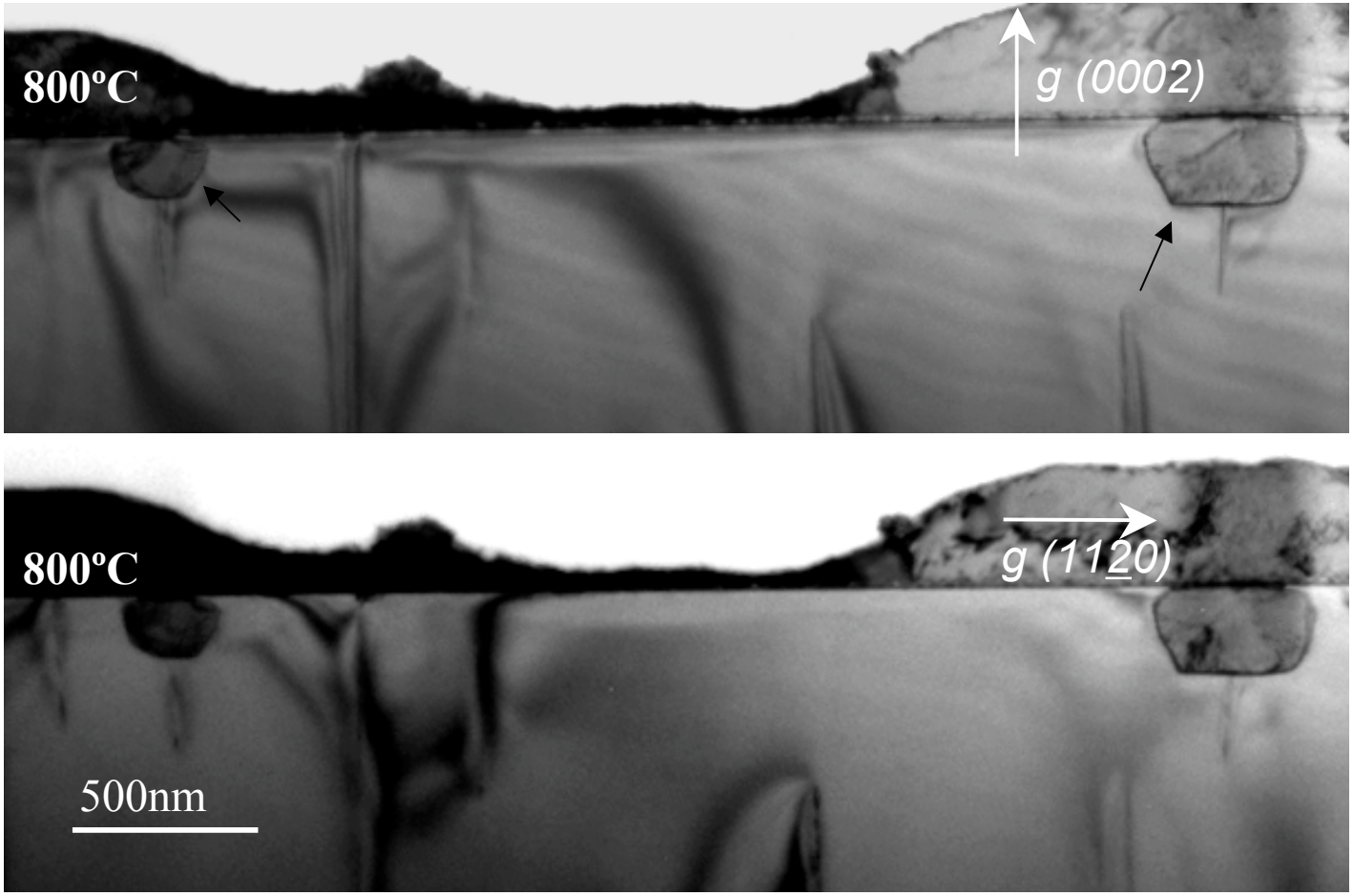

Screw + mixed

Edge + mixed

Two-beam diffraction-contrast TEM images from same area under different conditions.

- Most TDs inside GaN layer are edge- or mixed-type TDs.
- Contact inclusion density is less than the TD density.
- Most contact inclusions are associated with threading dislocations (TDs).

Contact inclusion: STEM and EDXS line profile

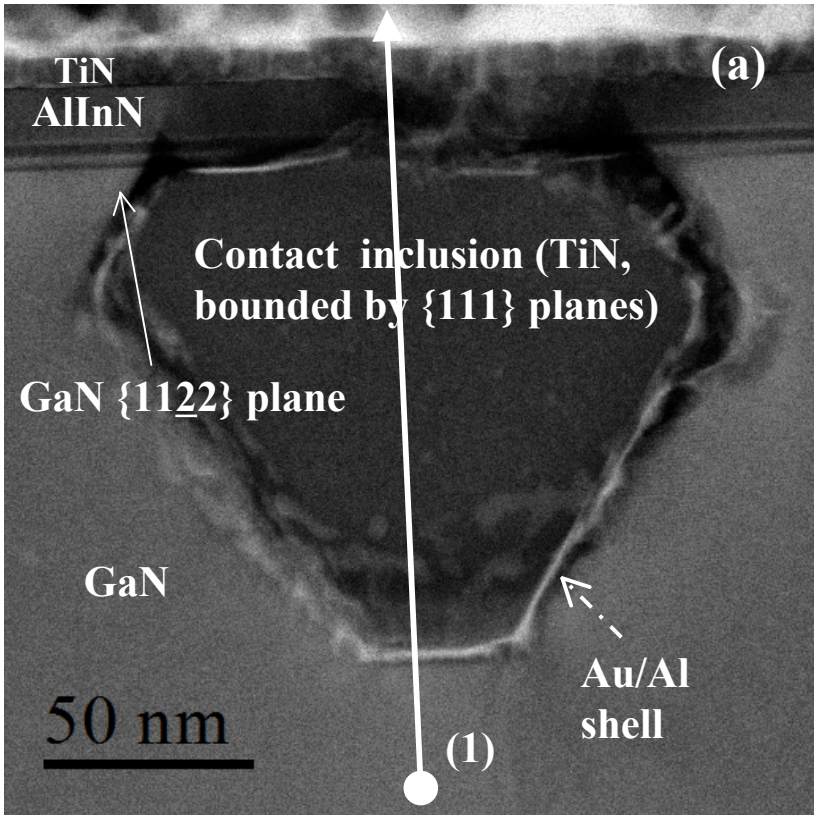

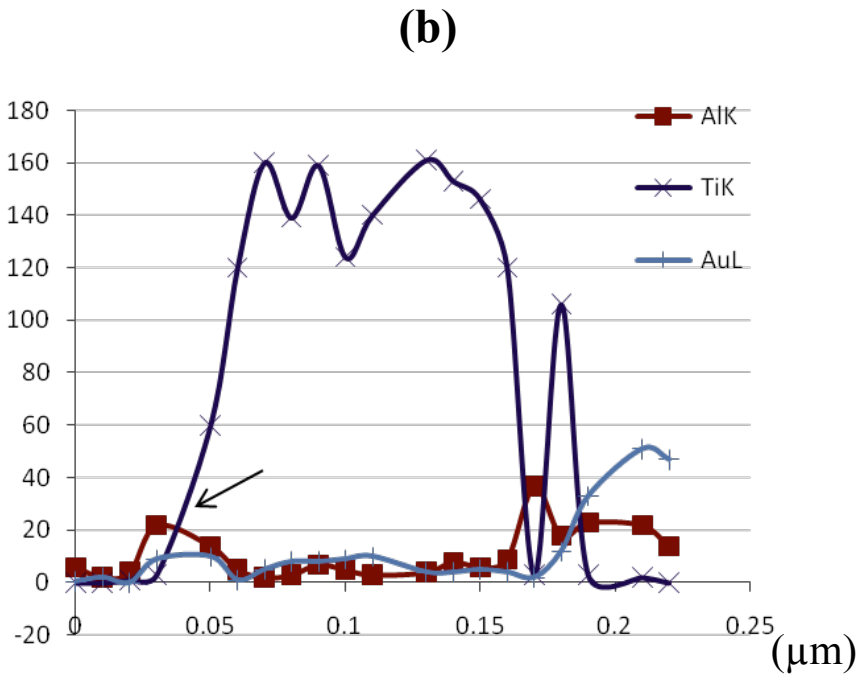

HAADF STEM image and corresponding EDXS line profile showing contact inclusions.

- TiN layer right above AlInN layer.
- Contact inclusions are mainly TiN.
- Inclusion has faceted shape (bounded by {111} planes) with surrounding Au/Al shell.

Contact inclusion: high-resolution TEM

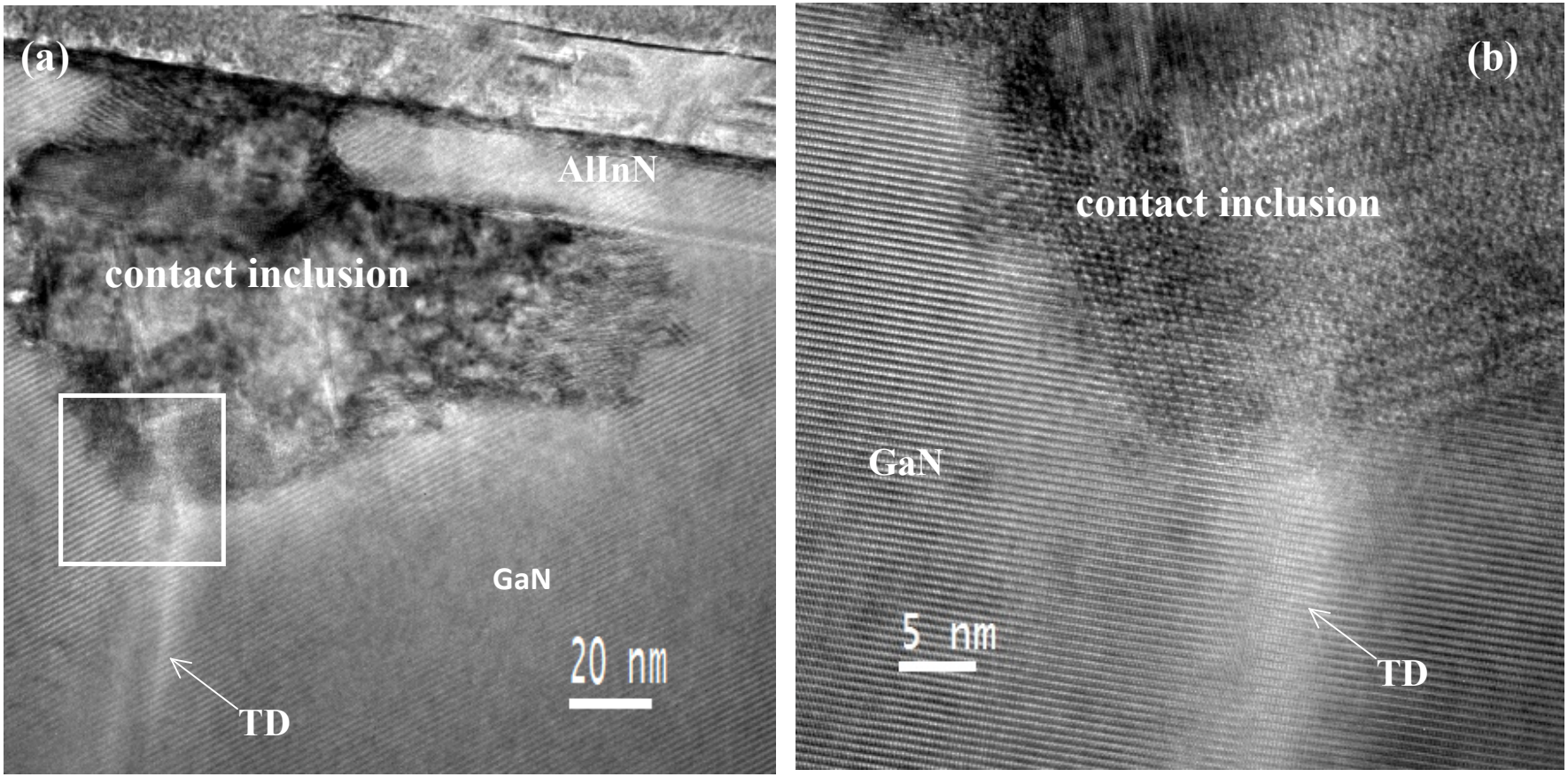

Higher magnification images taken at [11$\underline{2}$0] zone axis.

- Contact inclusions have ‘mushroom’ shape: larger inside the GaN layer.
- Contact inclusion has crystalline structure.

Role of contact inclusions

- Contact inclusions act as plugs through which carriers can flow between 2DEG and electrodes.
- Increase of TiN contact inclusion density will promote electron transport efficiency … but … it will also destroy part of the 2DEG interface and degrade device quality. Thus, an optimum contact inclusion density is required.

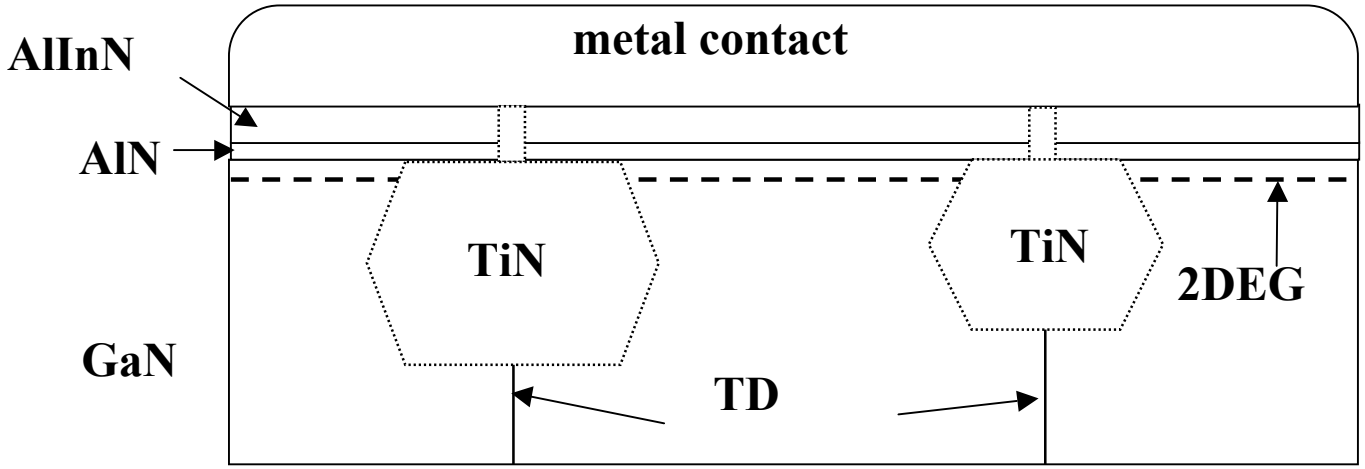

Zhou *et. al.*, JAP., 107 (2010) 014508.

Localized degradation in reverse-biased AlGaN/GaN HEMTs

Work in collaboration with A. Stocco, G. Meneghesso, and E. Zanoni (Padova)

Details of sample preparation

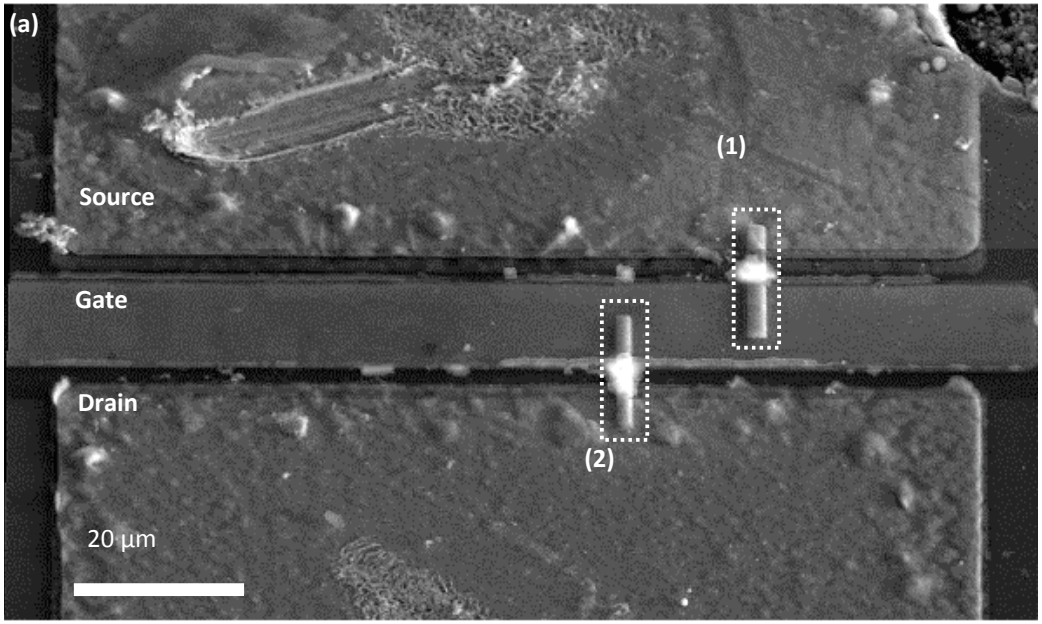

XTEM samples prepared at sites of 'hot spots' (1) and (2) which had previously identified by electroluminescence microscopy.

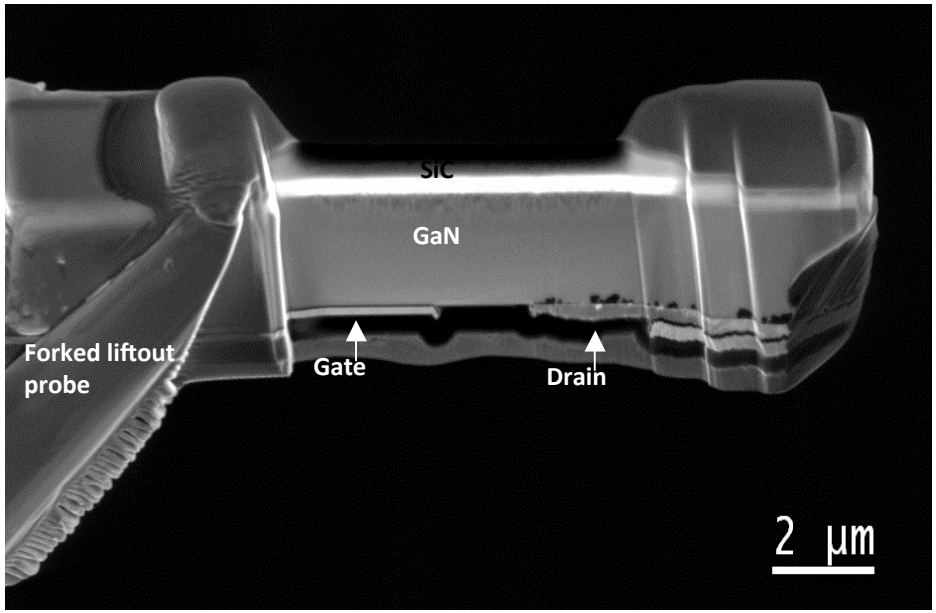

SEM image of FIB liftout from site of 'hot spot'. Backside milling used to minimize curtaining effects.

Examination of 'hot spot' region identified by EL

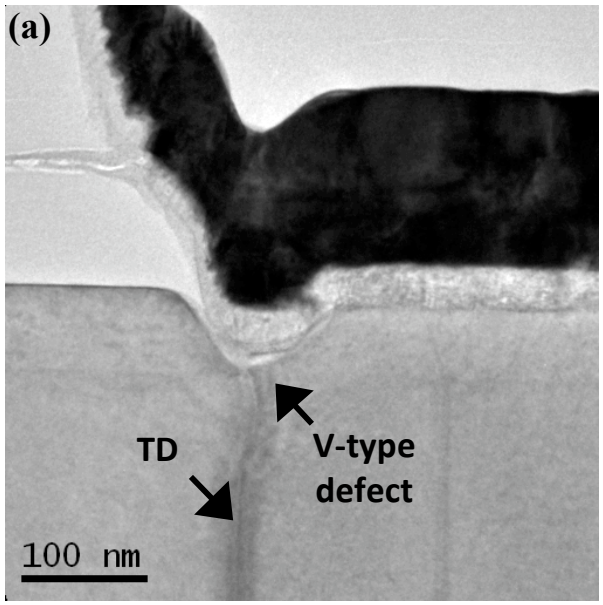

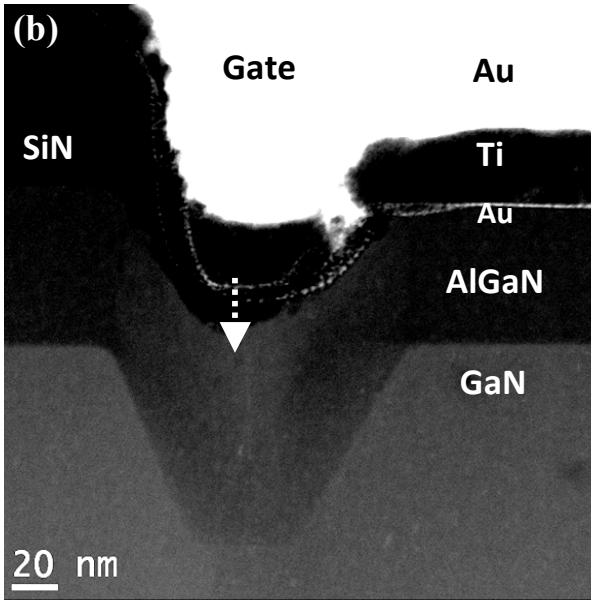

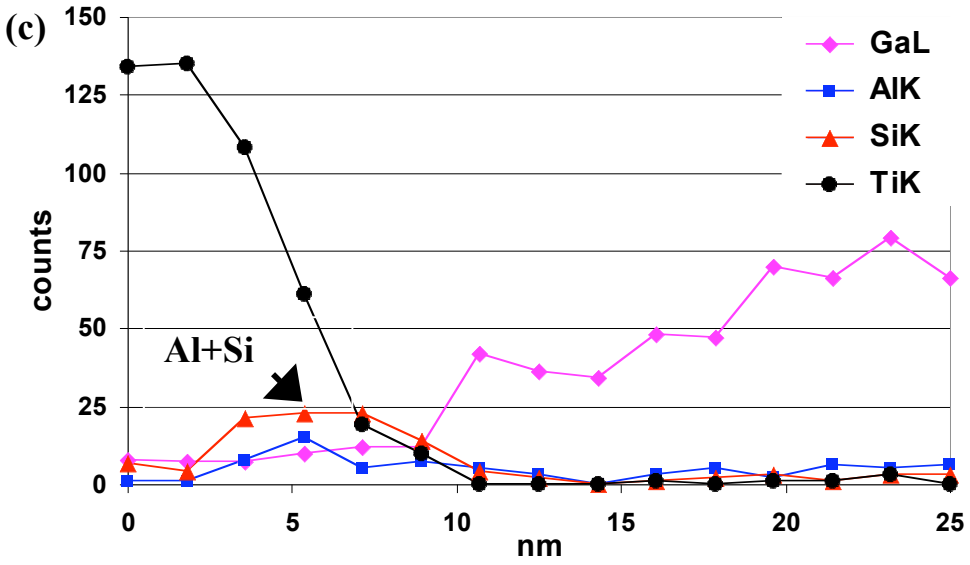

(a) BF image from region near gate edge showing V-type defect associated with a threading dislocation; (b) HAADF STEM image of same gate edge region; (c) EDX linescan along line indicated in (b) showing that cavity contains mixture of Au, Al, Ti, and Ga.

Examination of 'hot spot' region identified by EL

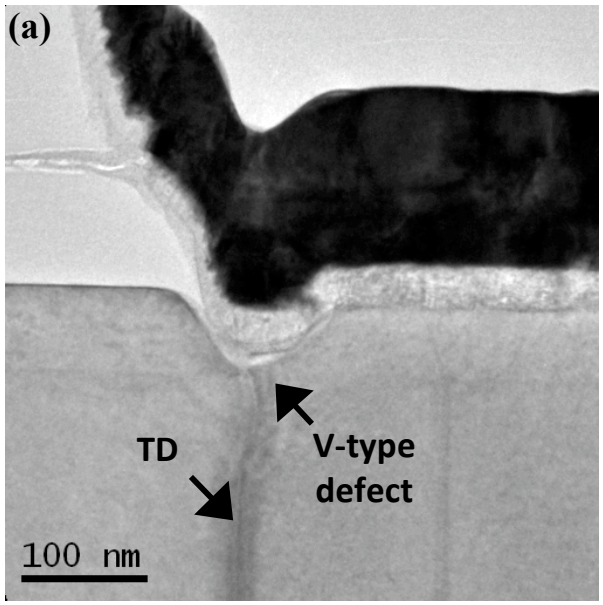

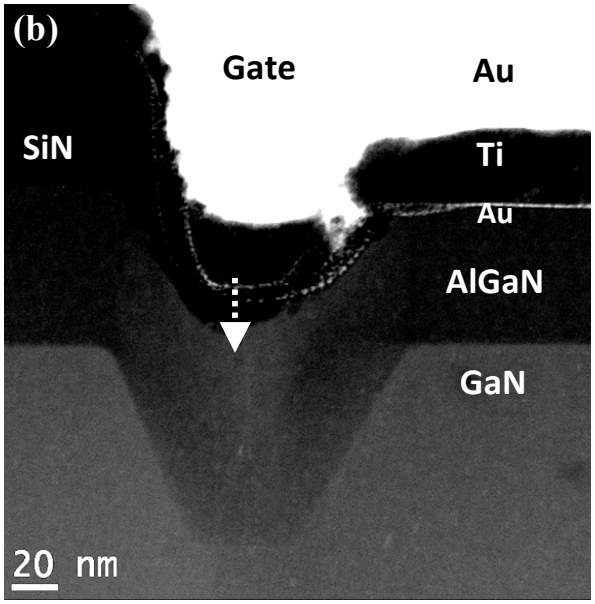

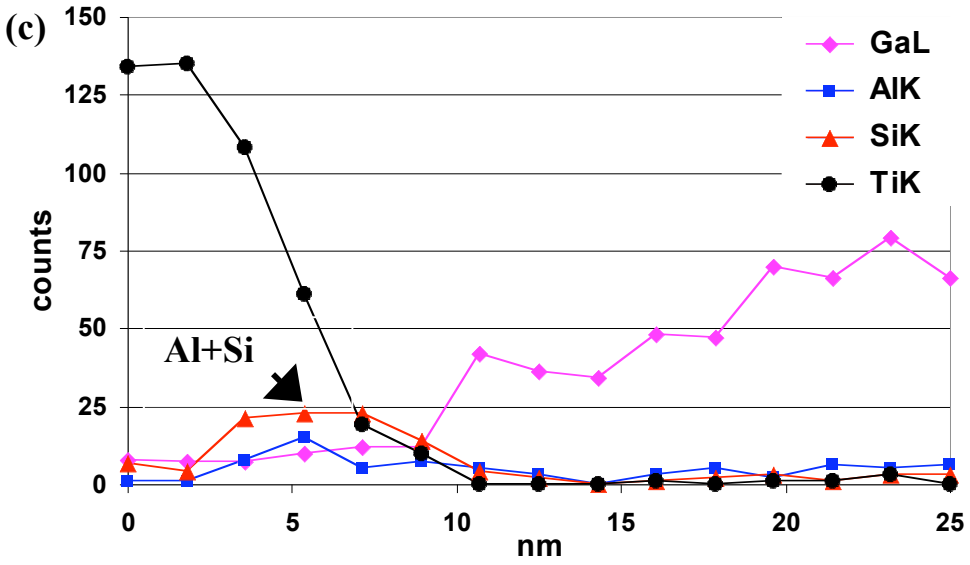

(a) BF image from region near gate edge showing V-type defect associated with a threading dislocation; (b) HAADF STEM image of same gate edge region; (c) EDX linescan along line indicated in (b) showing that cavity contains mixture of Au, Al, Ti, and Ga.

Unstressed device - pre-existing defect!

Stress-induced defect

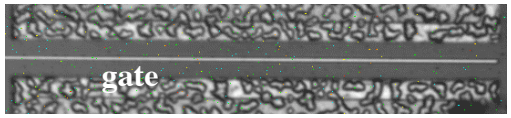

source
L_G= 0.5 µm, S46 wafer, unstressed
drain

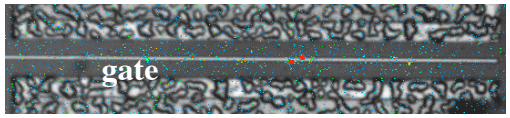

source
V_G= - 35 V
drain

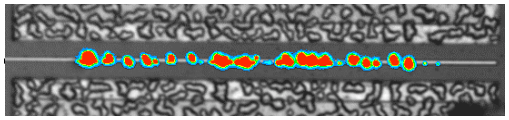

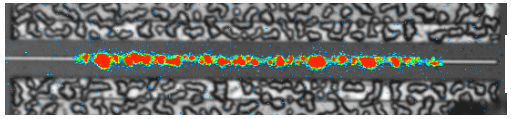

source
V_G= - 45 V
drain

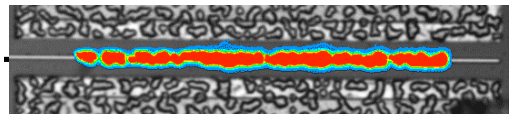

emission after test @V_G=-10 V, V_{DS}=0 V

emission during test

Series of EL images showing development of stress-induced defects.

Stress-induced ‘spike’ defect located 50nm from drain-side edge of gate.

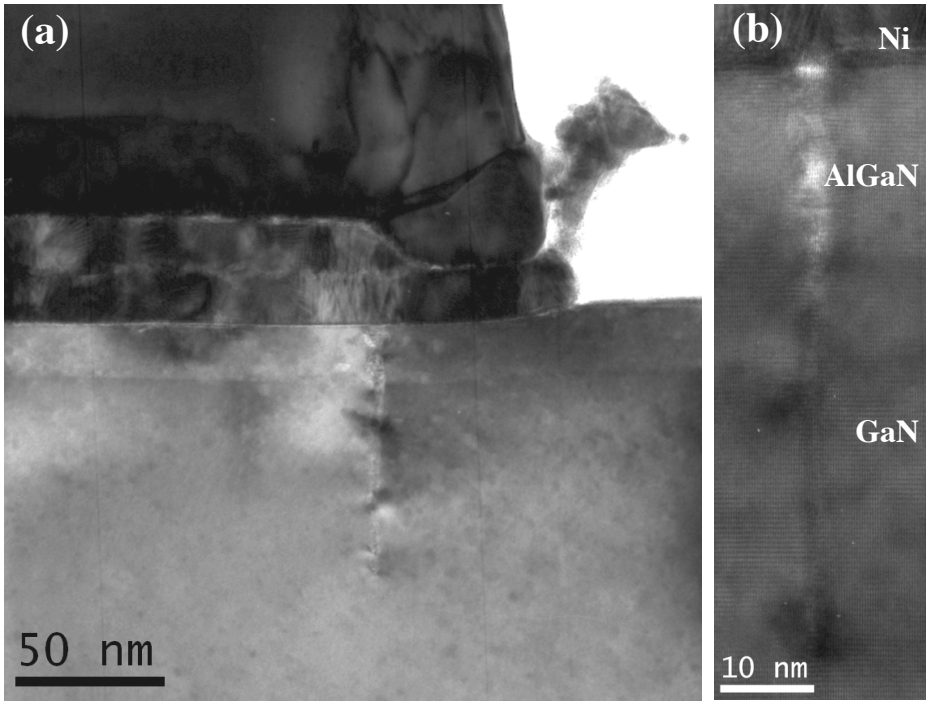

Examination of 'failed' region identified by EL

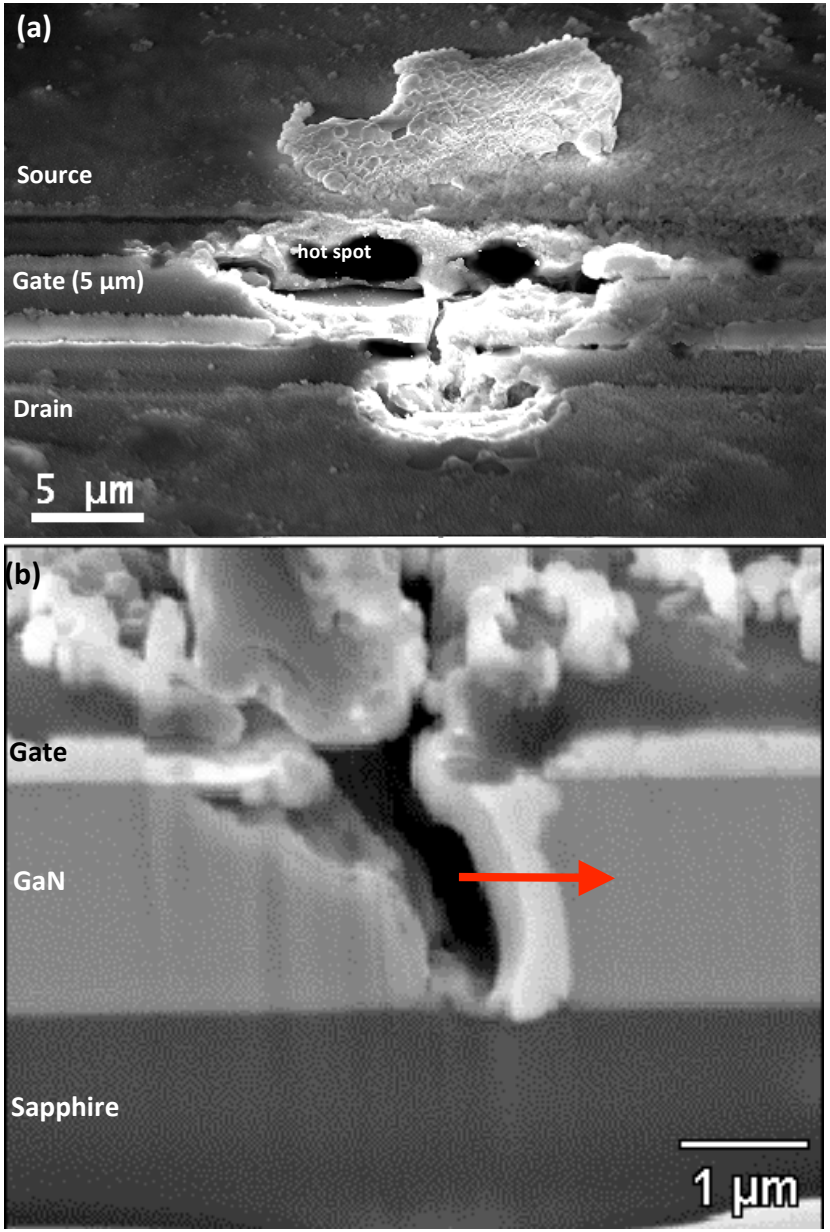

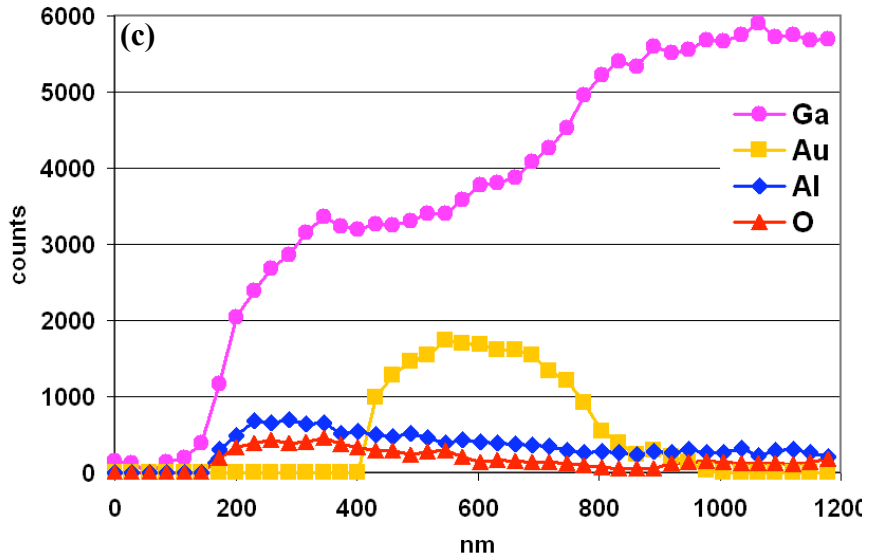

(a) SEM image of failed region during cross-sectioning; (b) Cross-sectional SEM image indicating that stress has originated at gate edge; (c) EDX linescan along line identifying Al_2O_3/Au bilayer coating wall beneath drain contact.

Effect of field plate - contd.

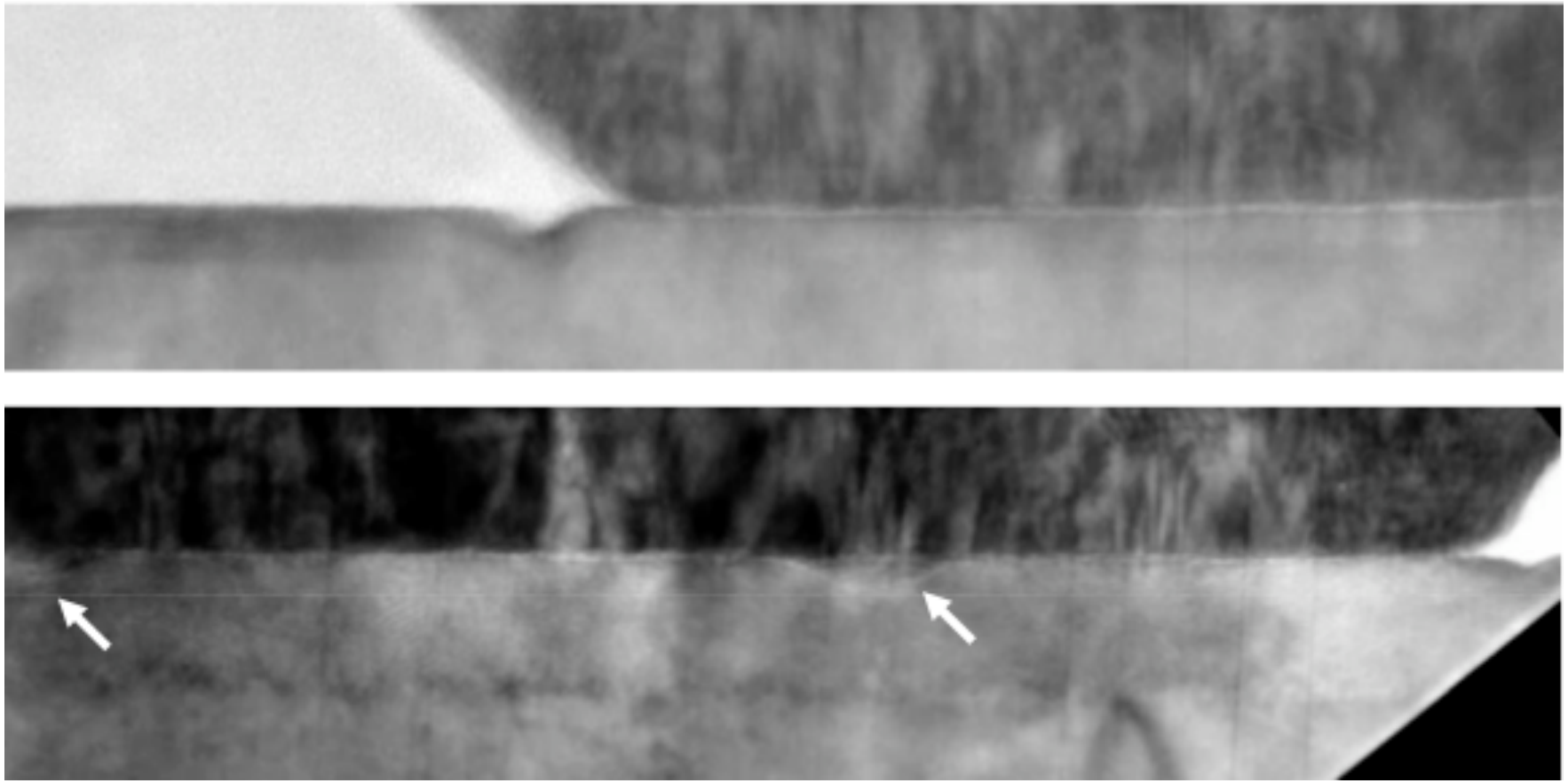

XTEM micrographs showing gate contact of off-state, step-stressed HEMT: (top) surface pit on *source* side of gate; (b) regions of Ni and oxygen diffusion (arrowed) on drain side of gate.

Liu *et. al.*, JVST B. 29 (2011) 032204

Effect of field plate - contd.

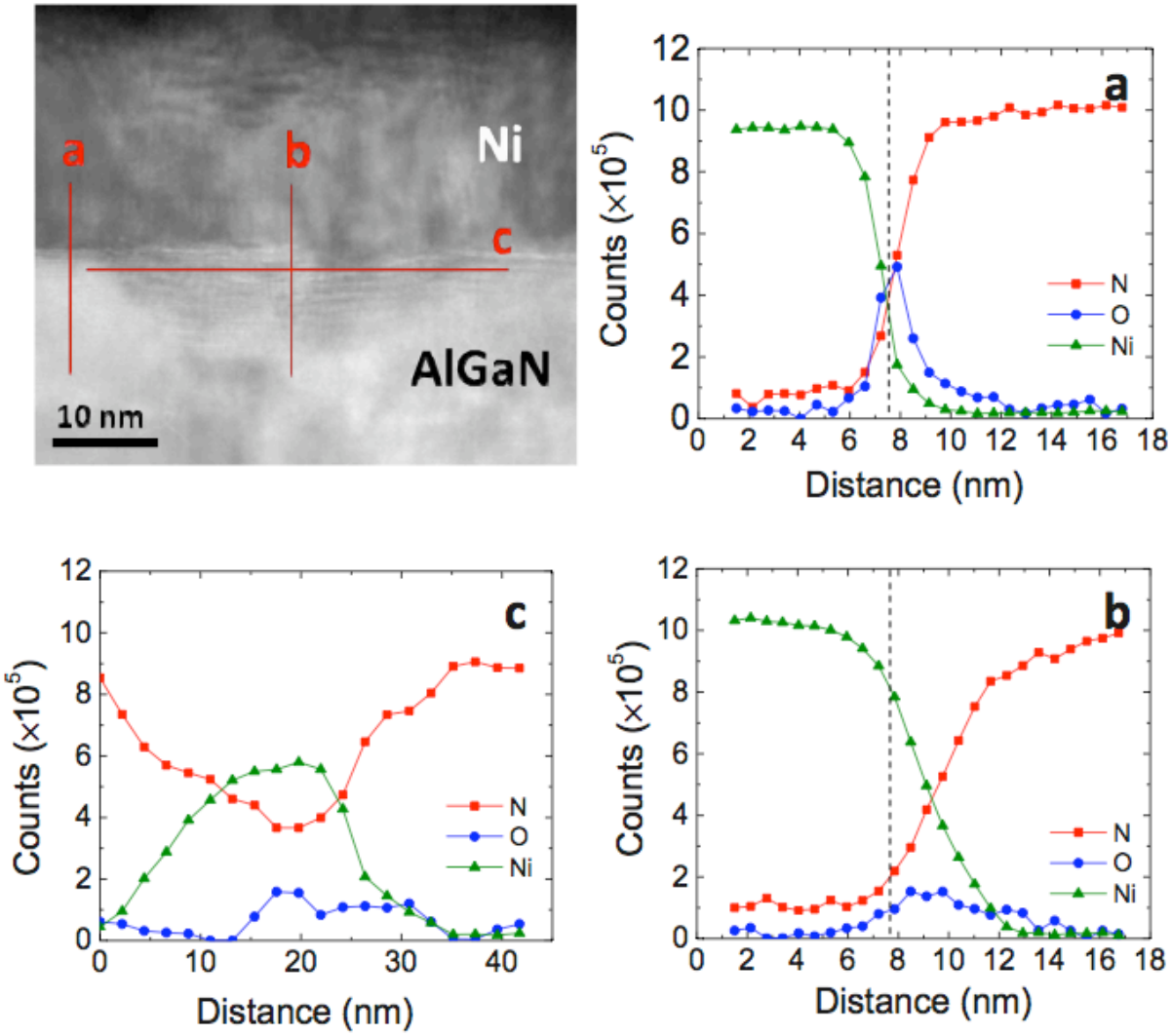

XTEM micrograph and EDX line scans showing Ni and O diffusion closely associated with threading dislocation.

AlInN HFET heterostructure

Work in collaboration with J.H.Leach, H. Morkoç (VCU)

Experimental details

- Metalorganic chemical vapor deposition on Al_2O_3.

- AlN buffer: 300nm
  - GaN (undoped): 3μm
  - AlN spacer: 1nm
  - AlInN: 13nm
  - GaN capping: 2 nm

- TEM sample preparation:
  - mechanical-polishing
  - low-energy ion-milling (liquid-N_2)

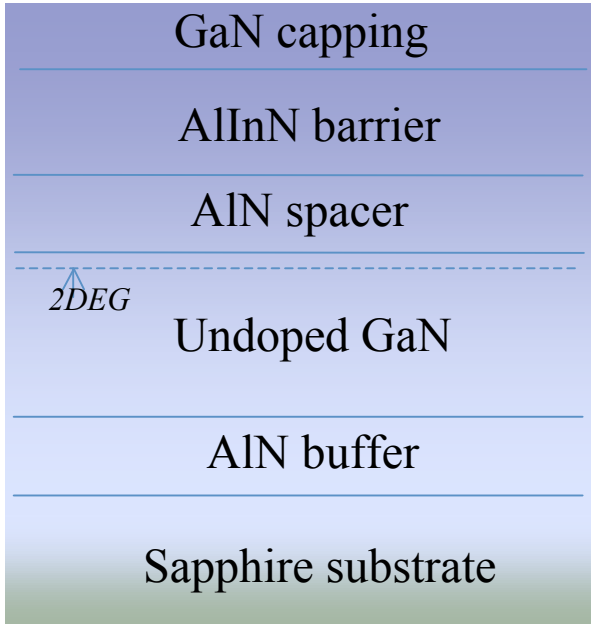

(not to scale)

JEOL 2010F was used for small-probe microanalysis, and a Philips CM200 FEG was used for holographic studies

HAADF STEM and EELS

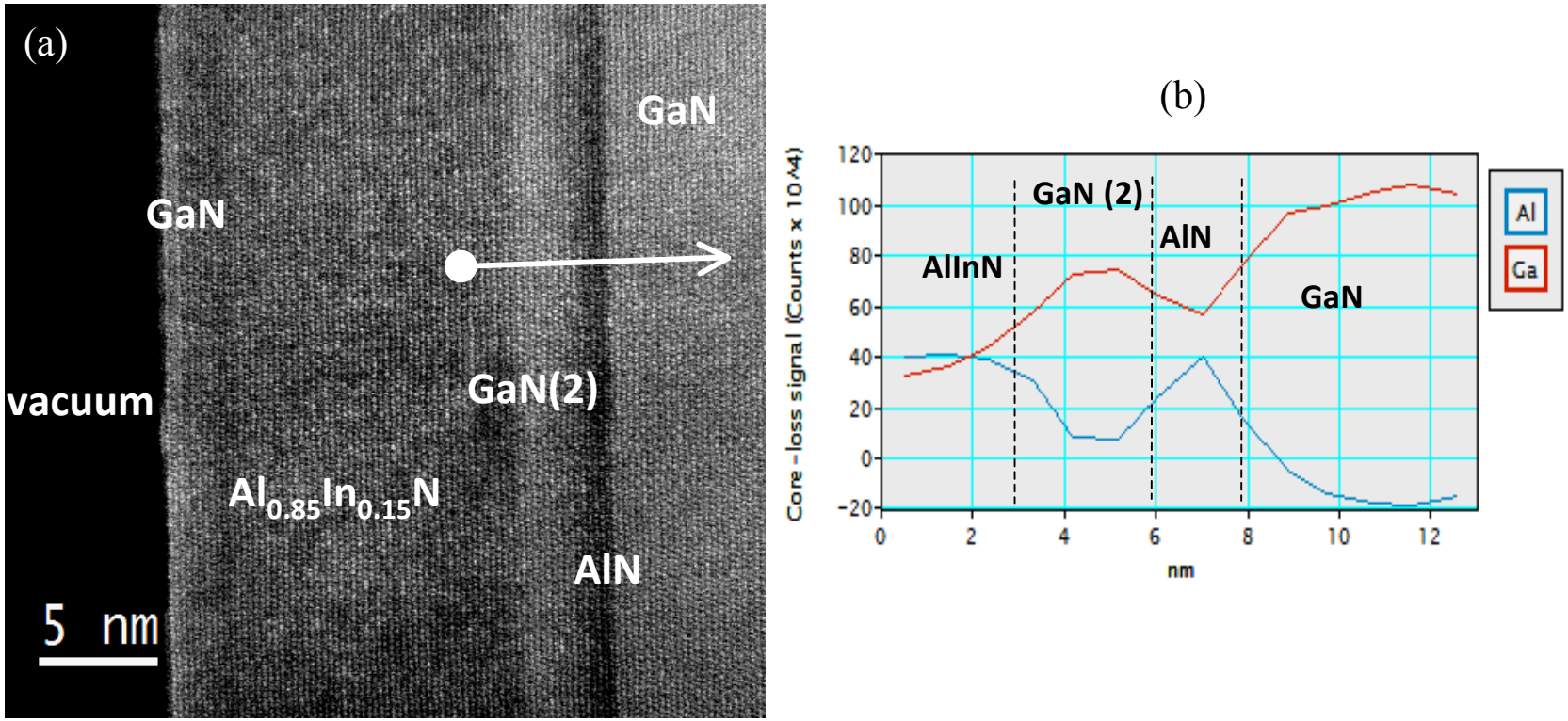

(a) HAADF STEM image, and (b) corresponding EELS line profile.

- Interfaces abrupt and well-defined.
- Unexpected Ga-rich layer between AlN and AlInN layers.
- Due to interruption of growth between AlN and AlInN layers, as needed when ramping down growth temperature.

Electron holography: polarization field and 2DEG

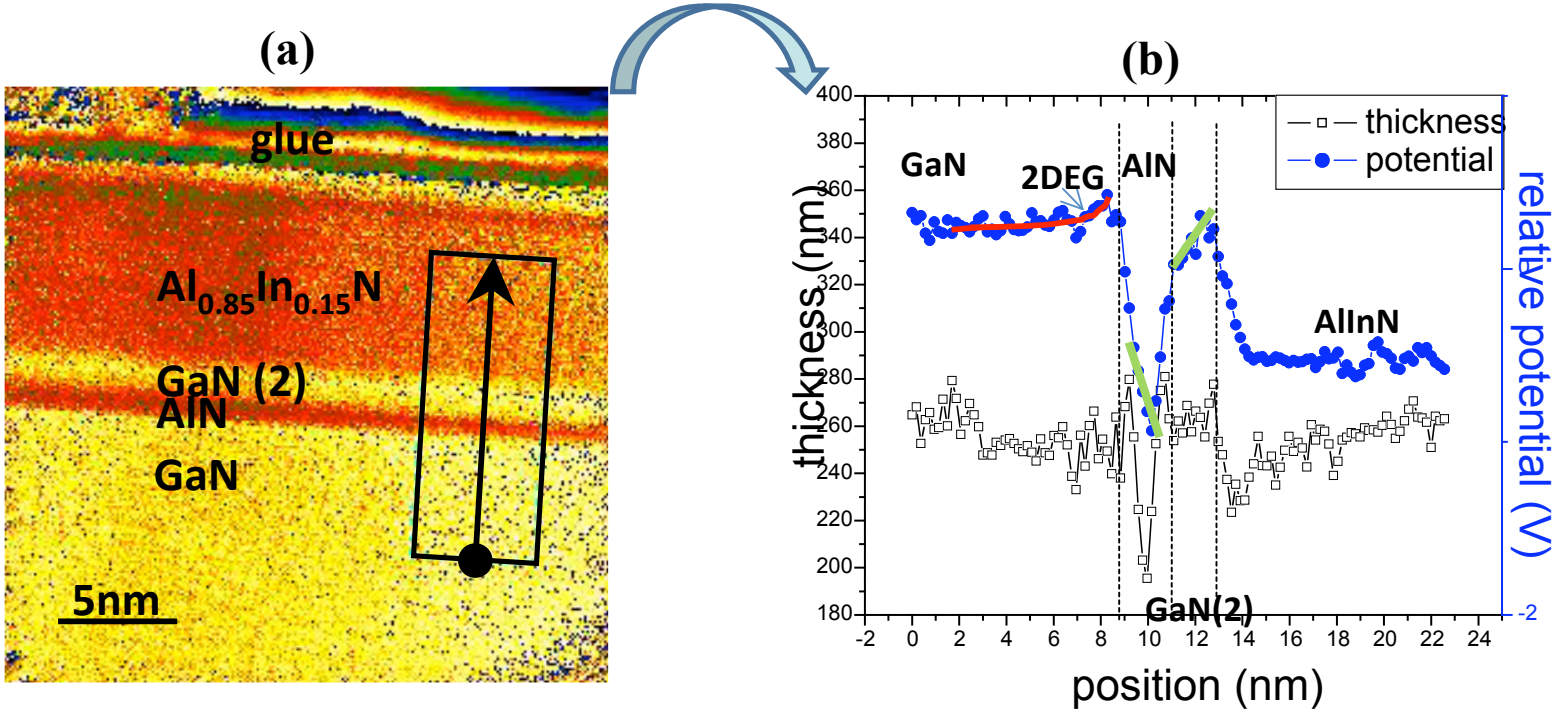

(a) Phase image; (b) Calculated potential and thickness profile.

E^{AlN} = 7.5MV/cm $E^{GaN(2)}$ = -2.2MV/cm

2DEG at GaN/AlN interface: **9.8×10^{12} cm^{-2}**

(without GaN(2) 2DEG: ~ 2.1×10^{13} cm^{-2}).

Leach, *et al.*, JAP, 107 (2010) 083706

Basis of off-axis electron holography

Nanoscale phase imaging of electrostatic and magnetic fields

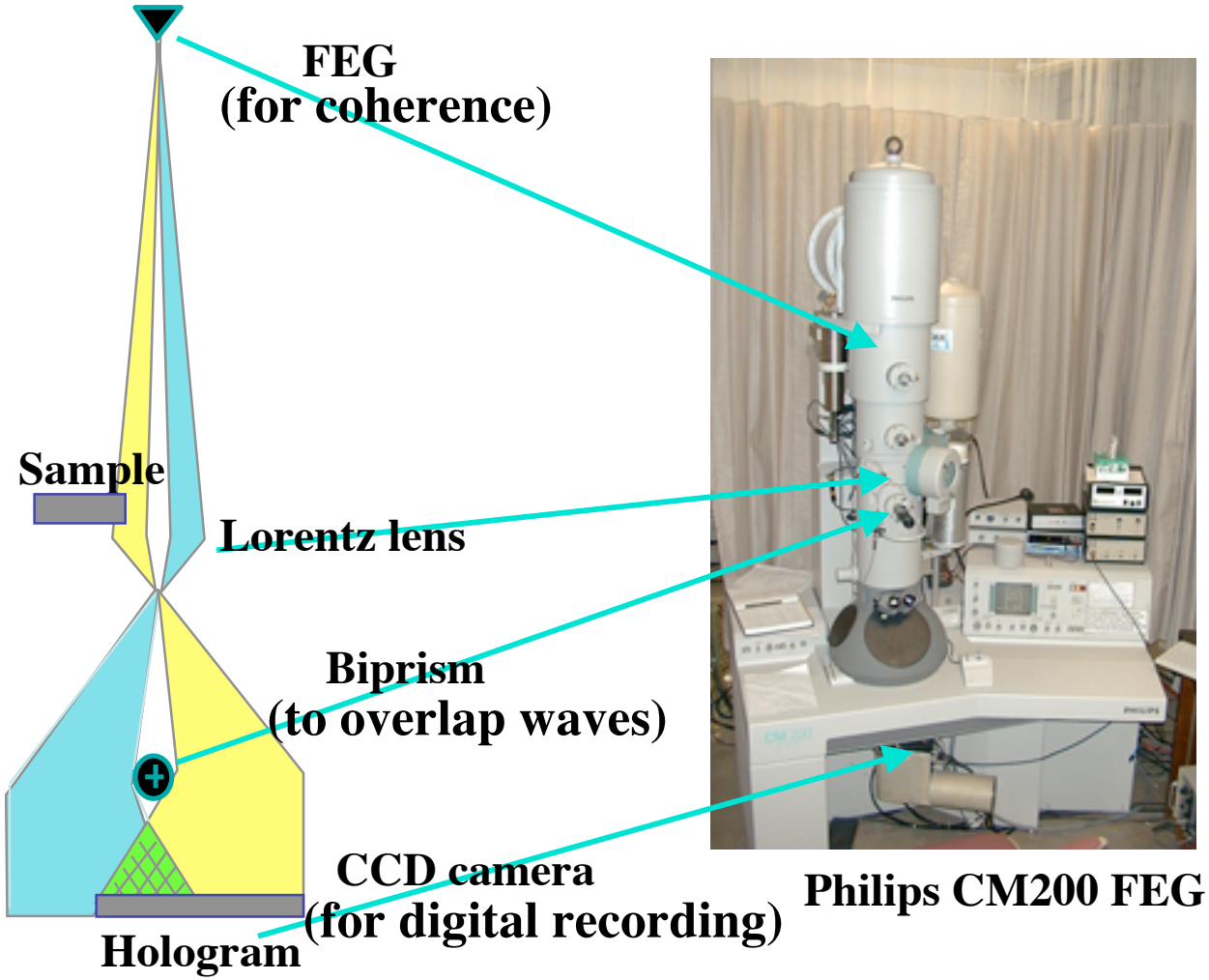

M.R. McCartney & D.J. Smith, Annu. Rev. Mater. Res. 37 (2007) 729

Electron holography for studying piezoelectric fields

Phase imaging at the nanometer scale

(a)

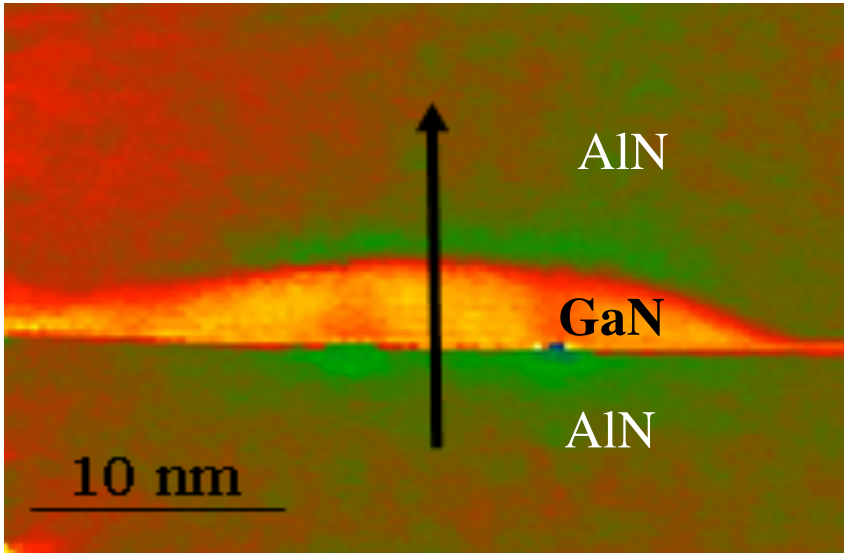

(b)

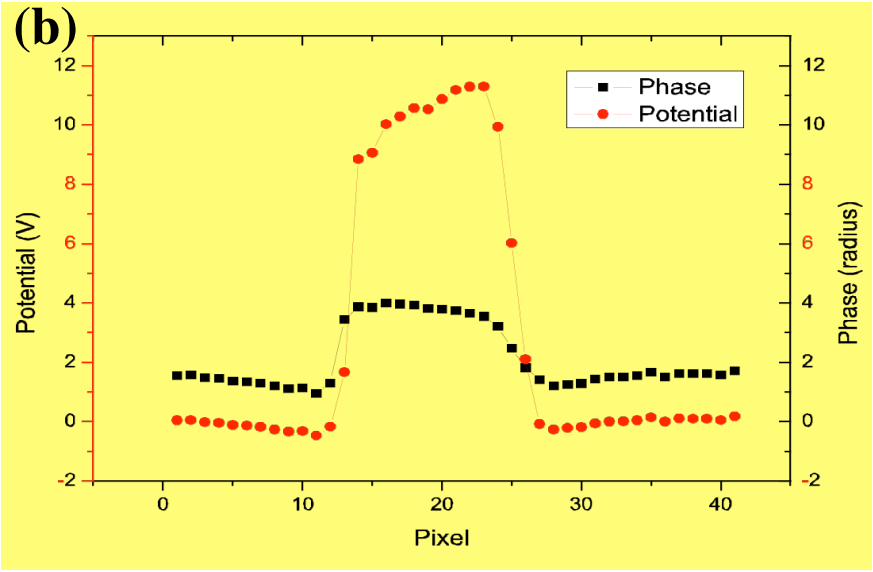

(a) Phase image from reconstructed hologram of wurtzite GaN QD with width of 32 nm and height of 4.5 nm.

(b) Corresponding phase profile (black line) and potential profile (red line) across center of GaN QD. Large phase shift observed inside QD. The electric field obtained by fitting slope of potential inside GaN QD is ~ 6MV/cm, consistent with theoretical calculations.

Similar methods are being used for studying biased HEMT devices

AlInN HEMT heterostructure

Polarization field mapping

Work in collaboration with A. Mouti, N. Grandjean (EPFL)

Morphology of $Al_{0.85}In_{0.15}N$/AlN/GaN HEMT

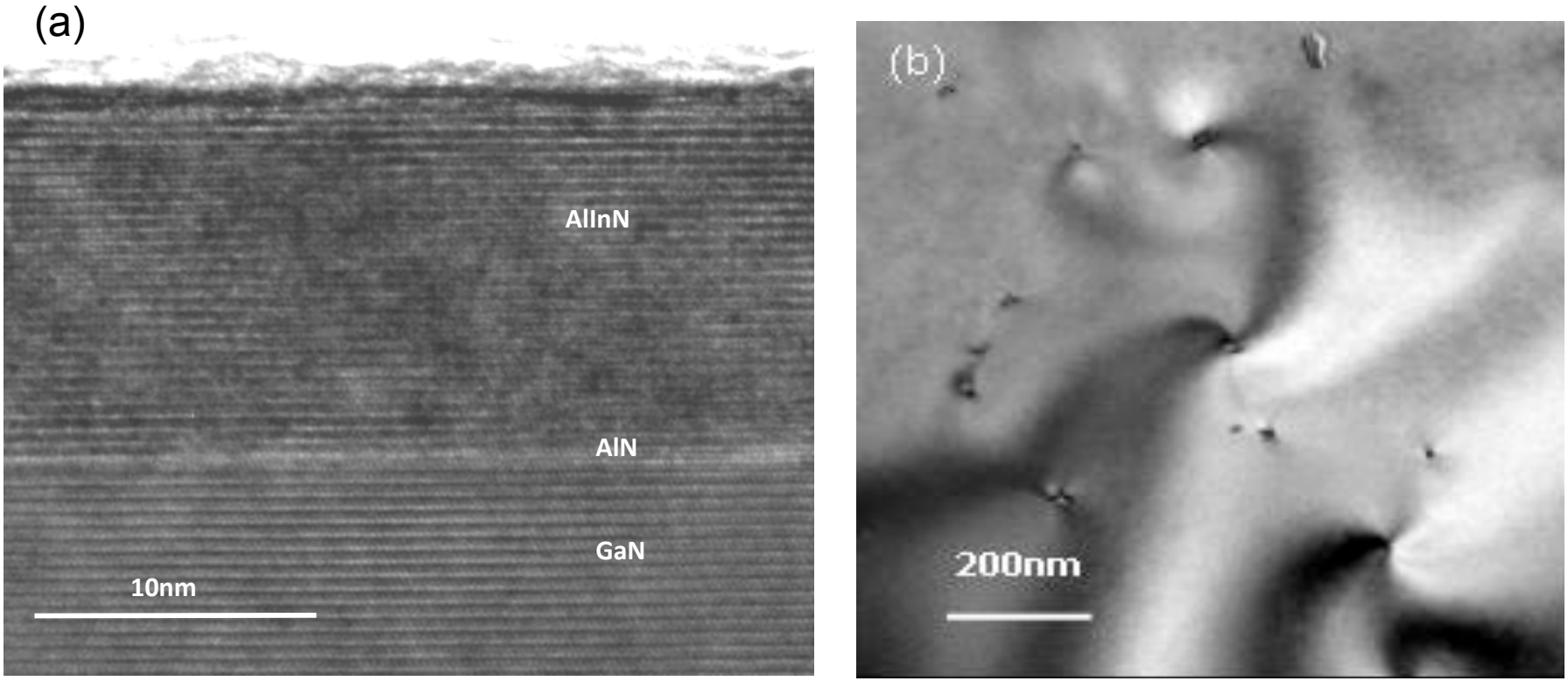

(a) Cross-sectional bright-field TEM micrograph of $Al_{0.85}In_{0.15}N$/AlN/GaN HEMT structure taken on [11$\underline{2}$0] zone axis shows well-defined and abrupt $Al_{0.85}In_{0.15}N$/AlN and AlN/GaN interfaces.

(b) Plan-view TEM image showing threading dislocations (TDs) in HEMT heterostructure. Estimated TD density ~ $9x10^{8}cm^{-2}$.

HAADF STEM and EDX line profile

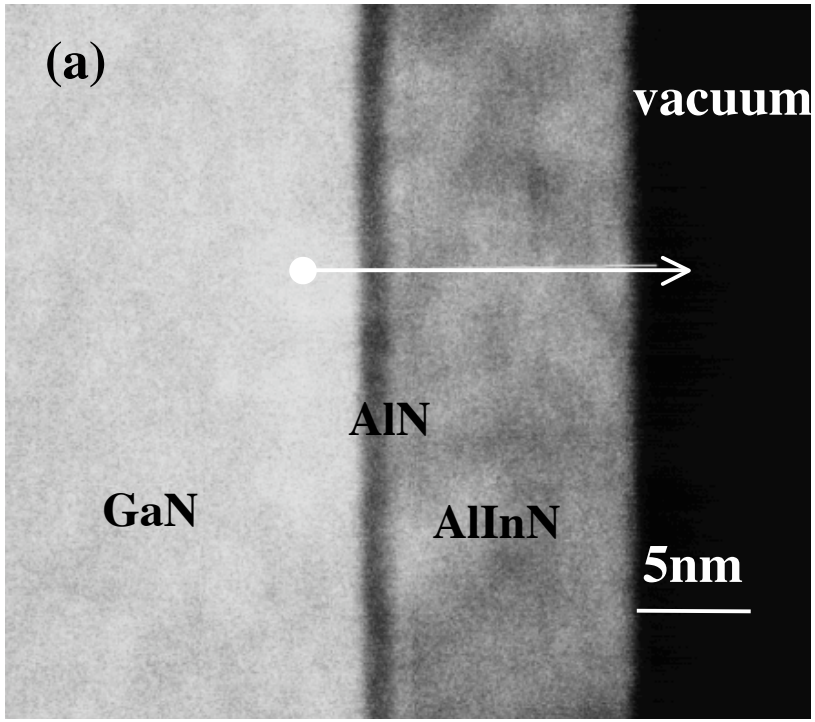

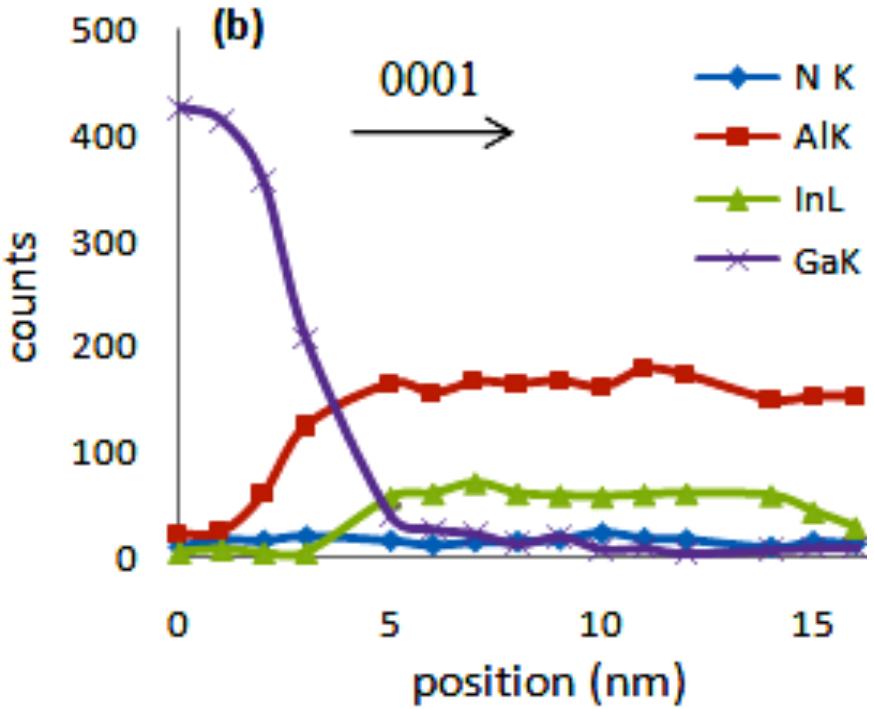

(a) HAADF STEM image of HEMT structure confirms abruptness of interfaces; (b) Corresponding EDX line profile shows uniformity of AlInN layer.

Electron holography: $Al_{0.85}In_{0.15}N$/AlN/GaN HEMT

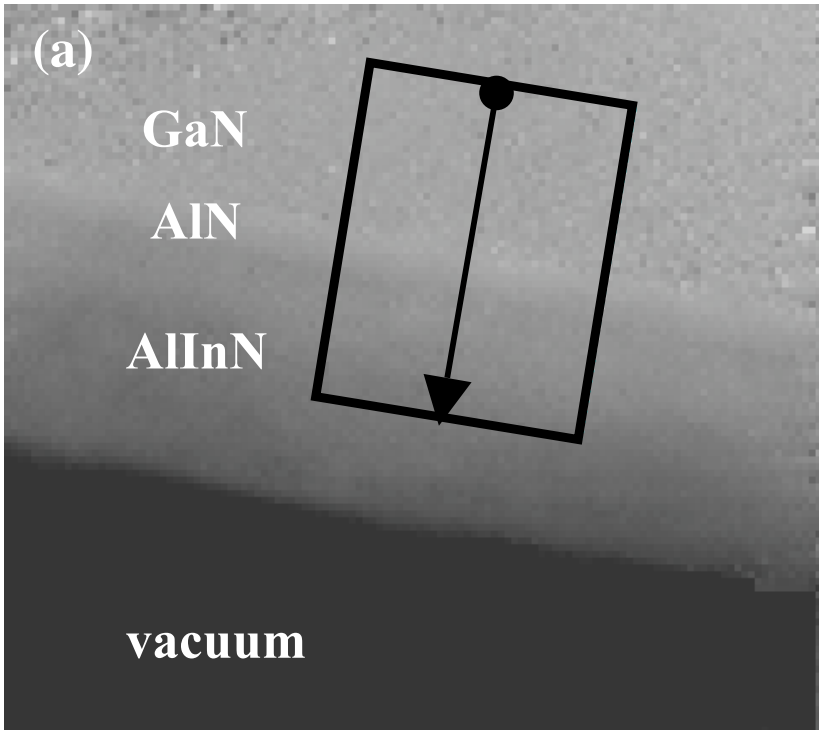

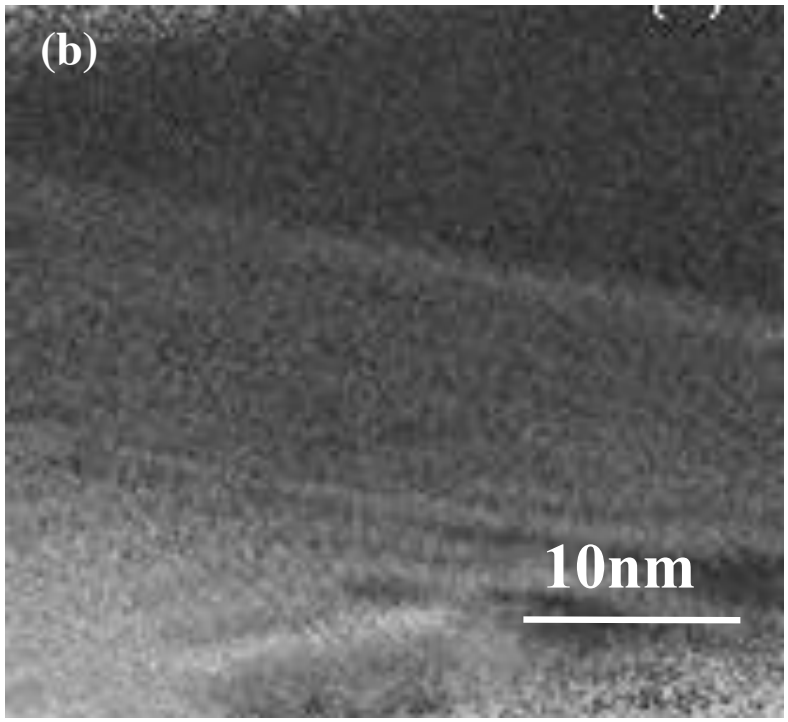

(a) Phase image, and (b) amplitude image, respectively, from reconstructed hologram of $Al_{0.85}In_{0.15}N$/AlN/GaN HEMT.

Electron holography: polarization field and 2DEG

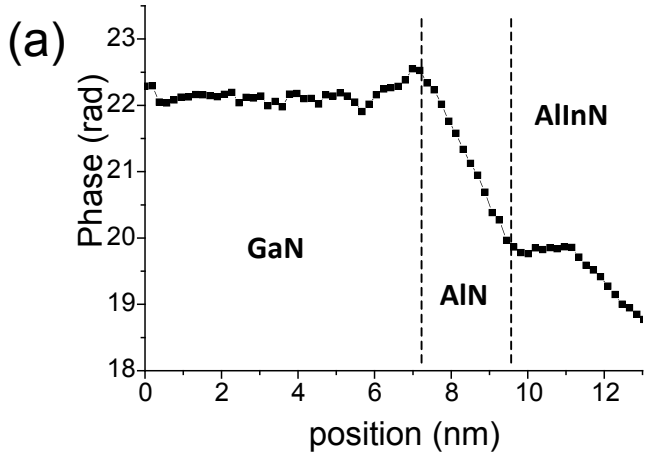

⊖⊕ : Polarization charge

− : 2DEG

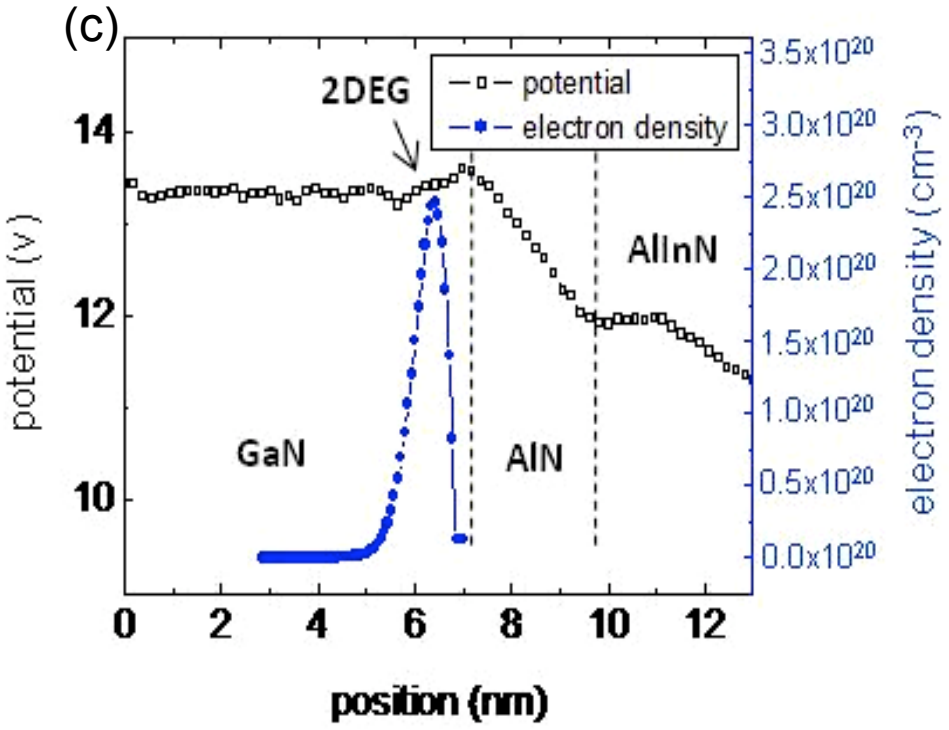

(a) Phase profile from phase image; (b) Schematic showing polarization charges and electric field near the AlInN/AlN and AlN/GaN interfaces; (c) Potential profile (open squares) and electron distribution (filled circles) across AlInN/AlN/GaN interface.

Electron holography: polarization field and 2DEG

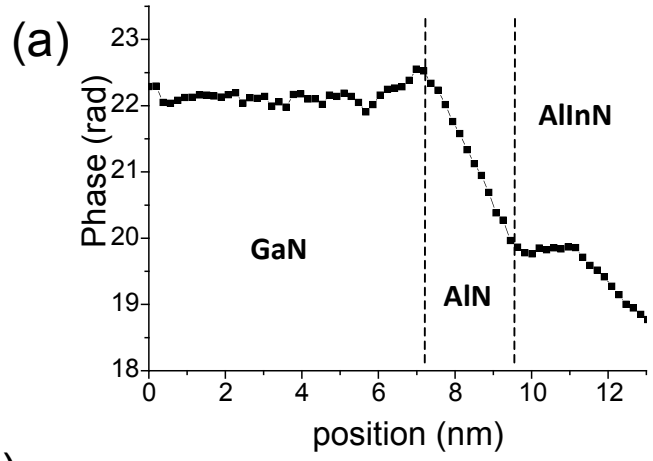

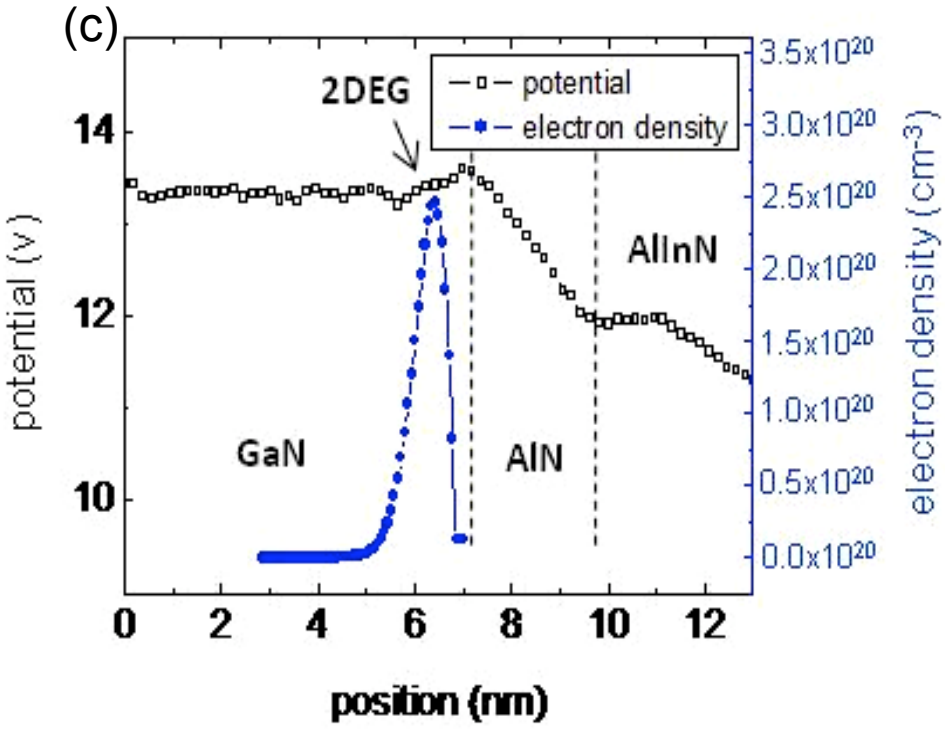

2DEG ~ 2.1x10^{13} cm^{-2}

E^{AlN} = 6.9 MV/cm

(a) Phase profile from phase image; (b) Schematic showing polarization charges and electric field near the AlInN/AlN and AlN/GaN interfaces; (c) Potential profile (open squares) and electron distribution (filled circles) across AlInN/AlN/GaN interface.

Zhou *et al*, APL, 94 (2009) 121909.

AlGaN/GaN HEMT heterostructure

Polarization field mapping

Work in collaboration with P.L. Fejes (Freescale)

Electron holography of AlGaN/GaN HEMT device

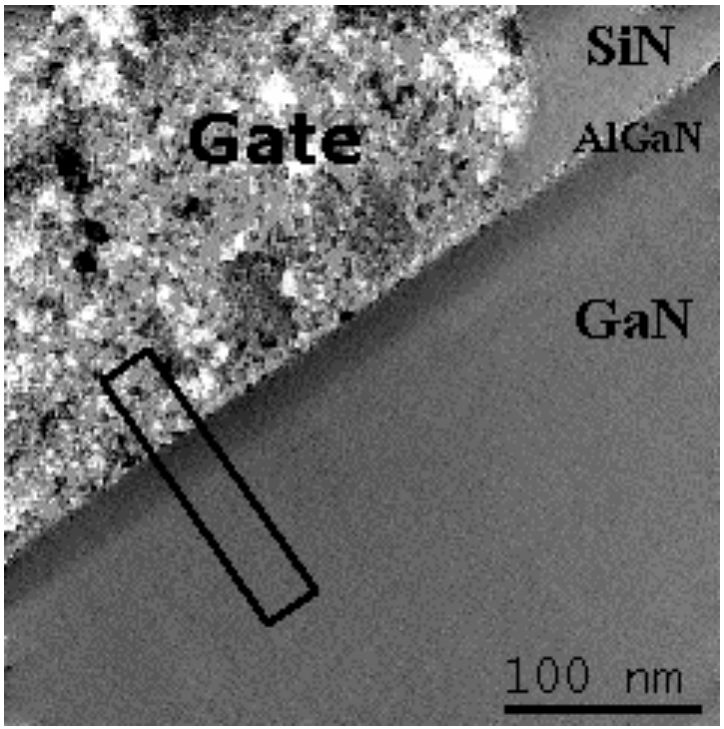

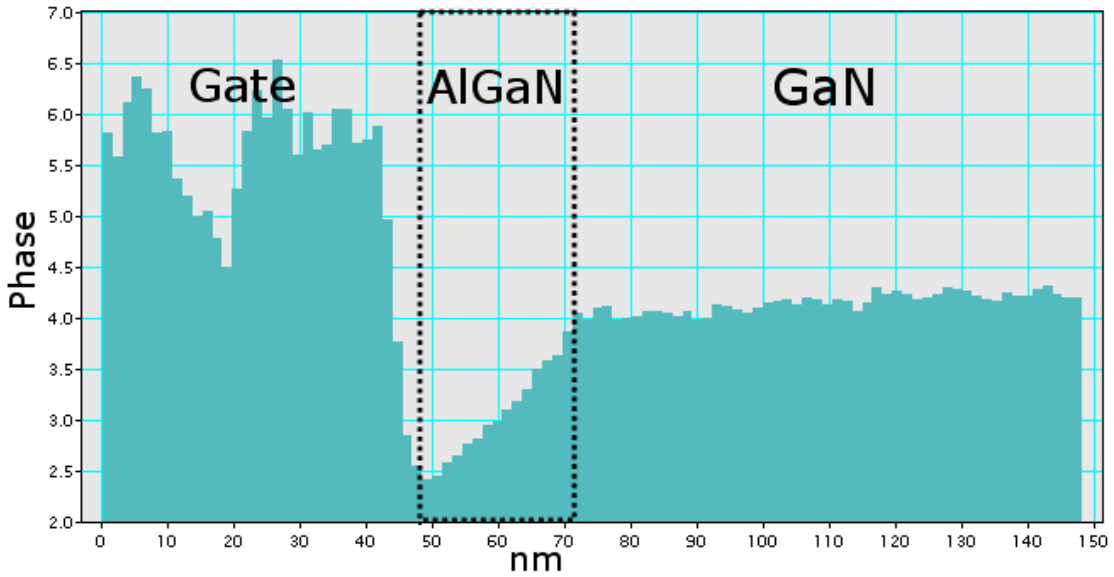

(Left) Electron holography phase image of AlGaN/GaN heterostructure in HEMT transistor device from region below the gate. (Above) Complementary phase profile. The slope of the phase in the AlGaN layer was used to quantify the intrinsic electric field arising from spontaneous and piezoelectric polarization.

- Reconstructed phase image shows distinct AlGaN layer
- Phase profile shows slope in phase across AlGaN
- Slope in phase directly proportional to internal electric field pointing towards the surface, E ~ 0.7 MV/cm
- Gate appears noisy because heavy Au/Ni atoms scatter electrons much more strongly.

Device Potential Profiles

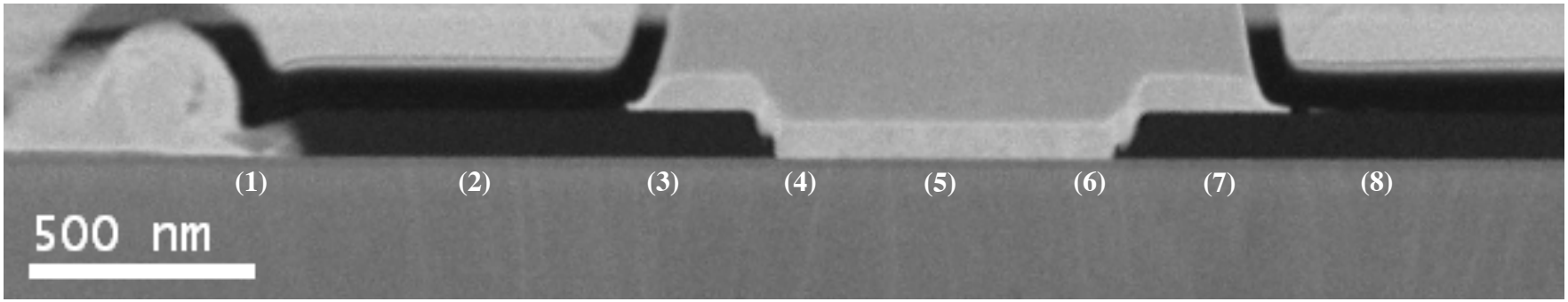

(Above) Z-contrast image of source and gate of AlGaN HEMT device prepared by FIB liftout.

(Below) Potential profiles across the AlGaN layer from several positions along the device. Each profile begins at the AlGaN surface, with each profile peak marking the AlGaN/GaN interface.

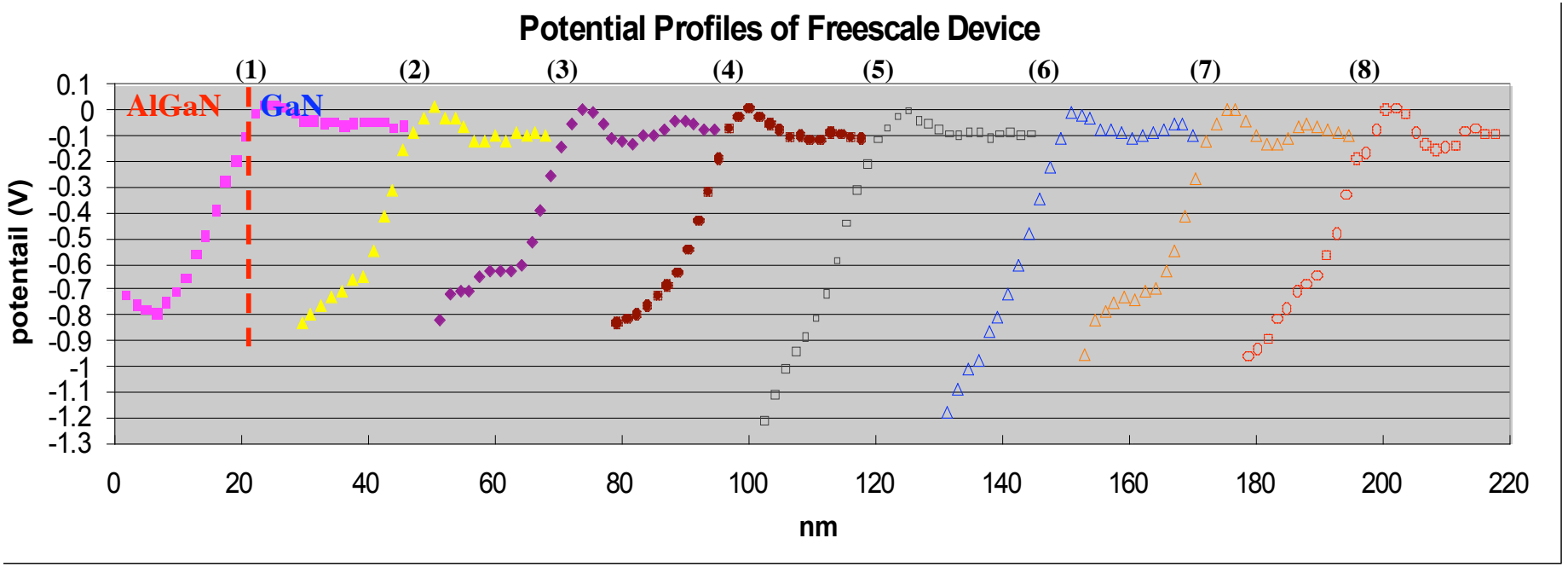

In Situ Biasing Experiments

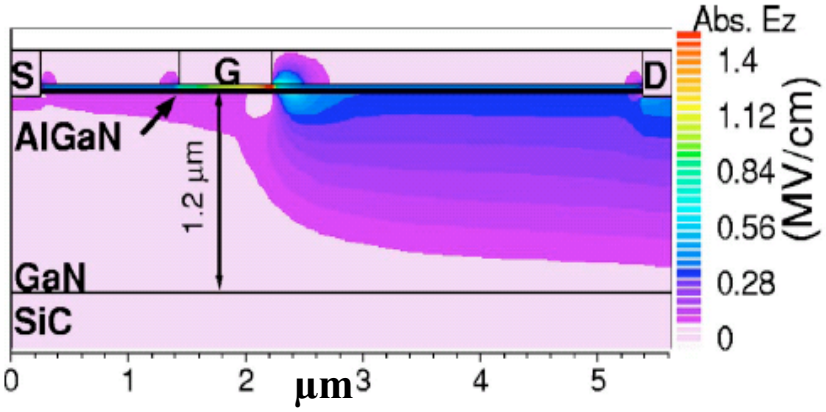

A. Sarua, et al., Appl. Phys. Lett. 88 (2006) 103502.

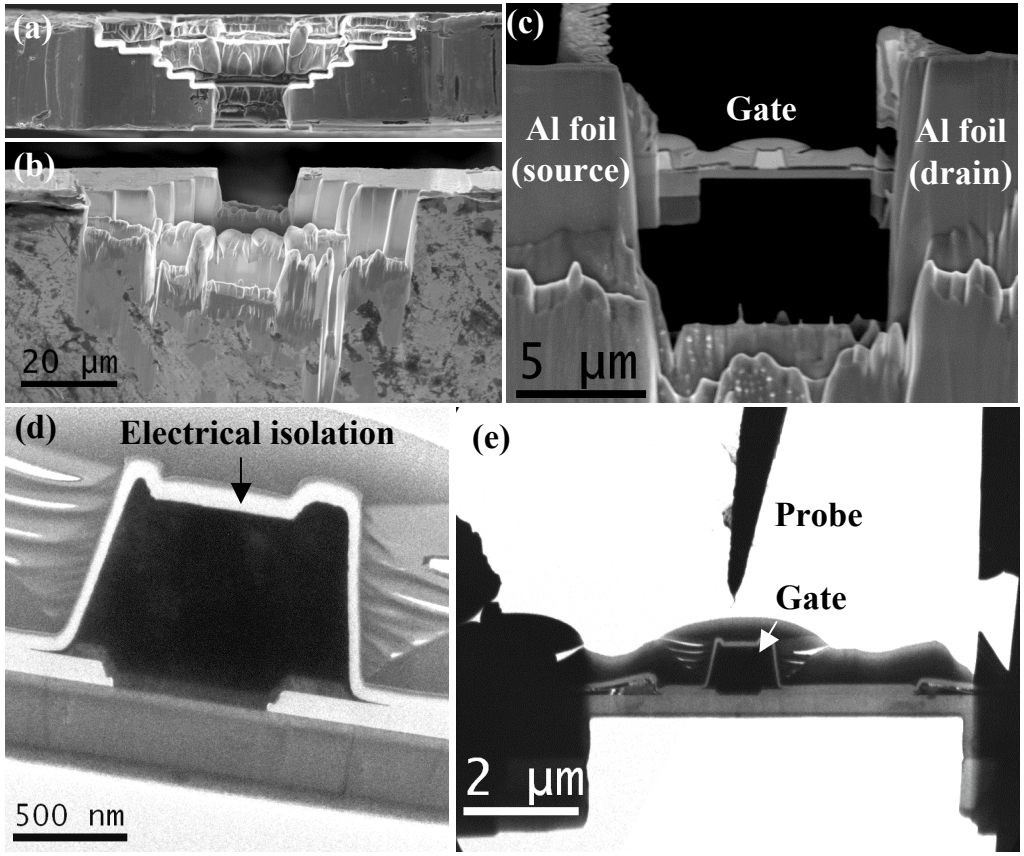

Experimental setup meant to mimic reverse-biasing step-stress tests.

Attach Al-foil to half Cu washer, cut mount into foil.

Transistor source and drain welded to Al foil using FIB-deposited Pt.

Electrical isolation between gate and source/drain.

Bias applied to source/drain, with gate grounded by moveable probe.

In Situ Biasing Experiments

Holograms recorded at gate edges under biased conditions.

Curtaining at gate edges complicated phase images.

Curtaining effects removed and effects of bias on profile emphasized by subtracting phase image recorded at 0 V from phase images recorded with applied bias.

I-V curves resemble diode, suggesting that FIB-damaged surfaces act as current leakage paths above threshold voltage.

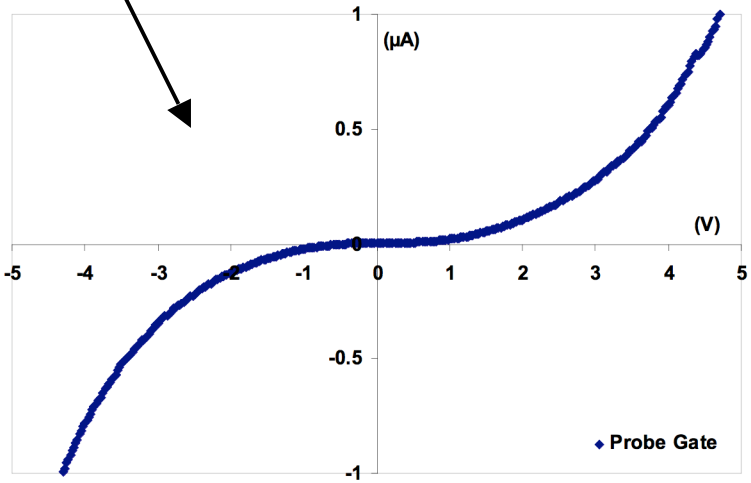

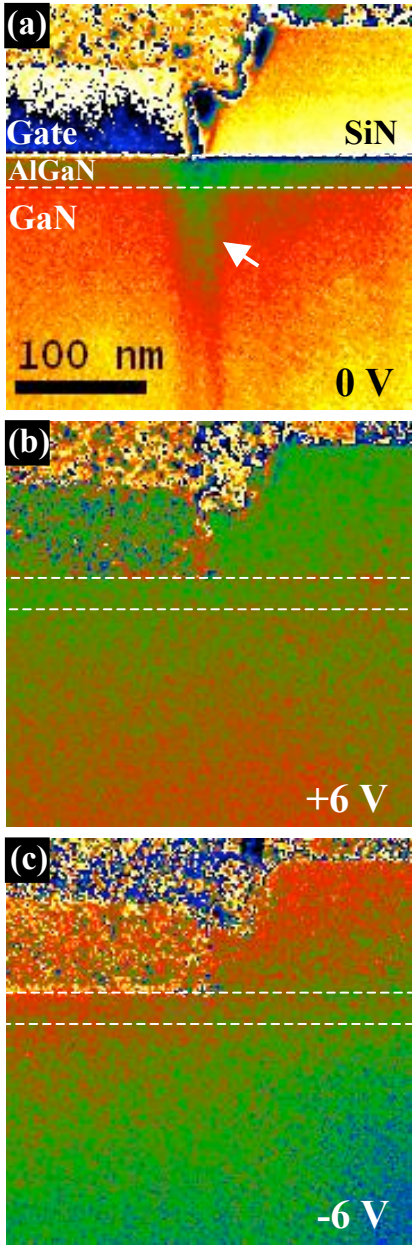

Conclusions

- FIB milling and liftout can be used to prepare entire HEMT cross-sections but care must be taken to avoid surface ion damage and sidewall implantation.
- Contact inclusions extend into AlN/GaN and AlInN heterostructure primarily along TDs, with density related to contact annealing temperature.
- Different morphologies observed for contact inclusions in AlGaN/GaN and AlN/GaN HEMT devices.
- Observation of 'hot spots' previously identified by electroluminescence microscopy suggest different possible failure mechanisms.
- Electron holography measurements of GaN/$Al_{0.85}In_{0.15}N$//GaN(2)/AlN/GaN HFET showed polarization-induced fields of 7.5MV/cm, and 2.2MV/cm, within AlN, and Ga-rich layers, respectively.
- *In situ* biasing experiments remain a 'work in progress'

david.smith@asu.edu molly.mccartney@asu.edu

Smith, *et al*. Micro. Reliab. 50 (2010) 1514

Surface and sidewall damage during FIB preparation

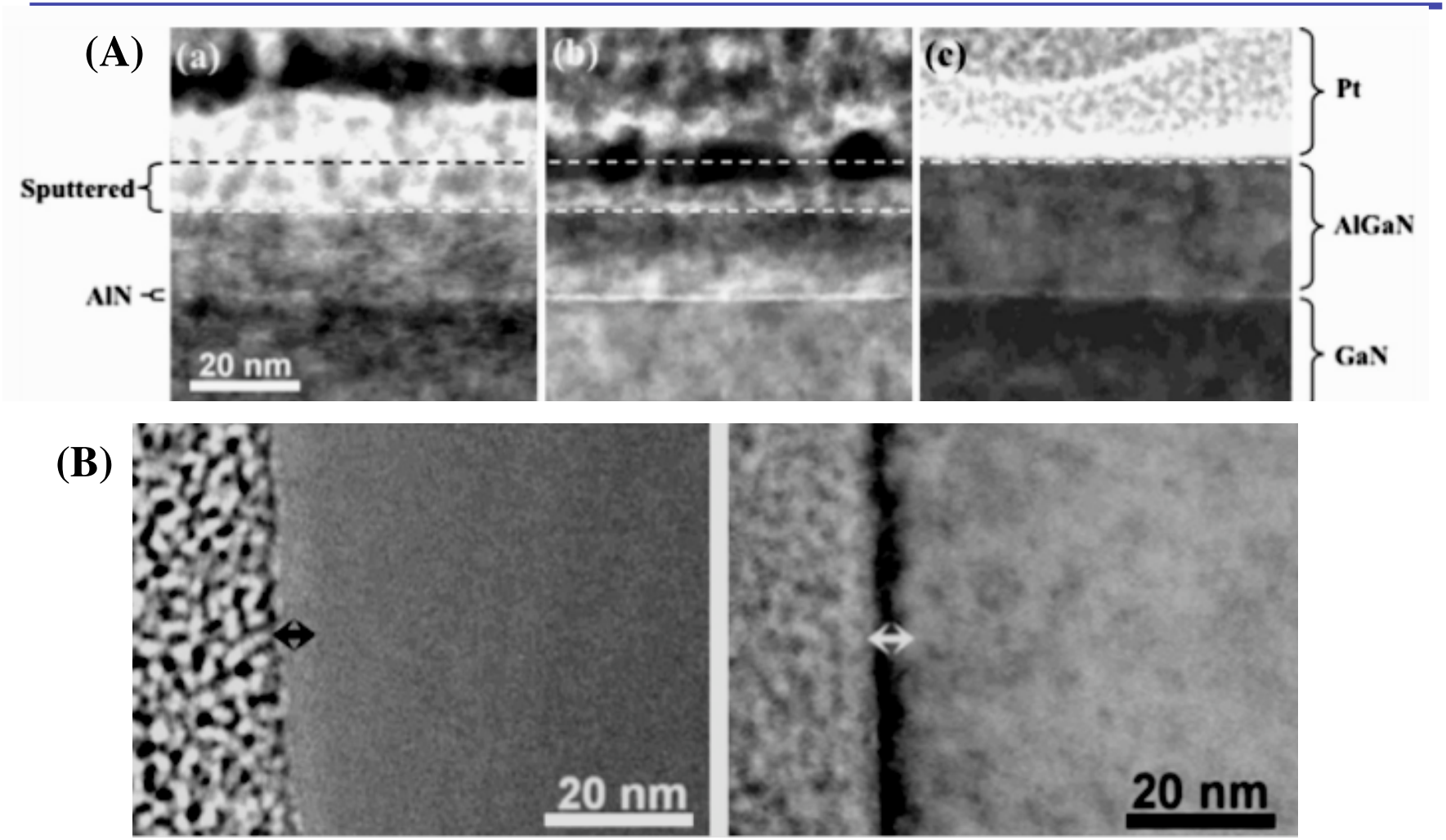

(A) XTEM micrographs of AlGaN/AlN/GaN HEMT structure showing extent of *surface damage caused during Pt deposition*: (a) 30-keV Ga ion beam; (b) 5-keV Ga ion beam; and (c) 30-keV e-beam. (B) (left) DF, and (right) BF images showing extent of *Ga-ion sidewall implantation* due to FIB milling with 2-keV ion beam.

Cullen and Smith, JAP, 104 (2008) 094304

TEM methods for characterizing HEMT devices

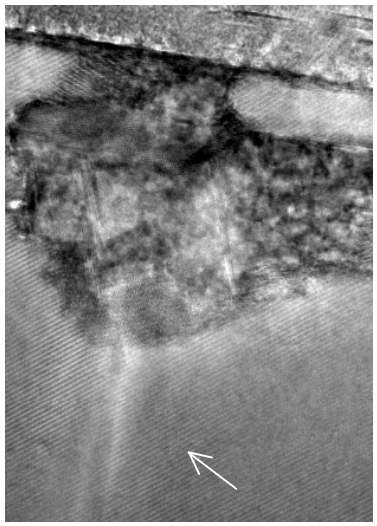

TiN contact inclusion for AlInN HFET

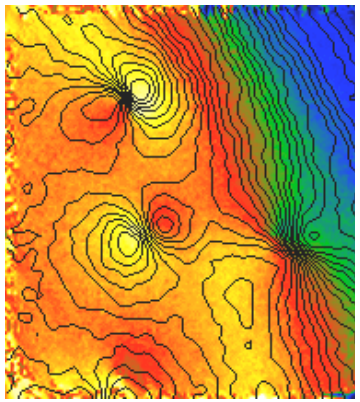

Phase image of InGaN TDs

Advanced TEM techniques

* **transmission electron microscopy**
  - **cross-sectional imaging of thin films and nanostructures**
  - **characterization of defect microstructure**
* **(aberration-corrected) atomic-resolution electron microscopy**
  - **direct imaging of atomic arrangements at defects and interfaces**
  - **chemical lattice imaging *and* geometrical phase analysis**
* **convergent beam electron diffraction**
  - crystallographic analysis
  - **local lattice parameter determination**
* **(aberration-corrected) scanning transmission electron microscopy**
  - **"Z"- contrast imaging**
  - nanoprobe diffraction
* **nanospectroscopy**
  - **determination of local composition**
  - **comparison of chemical sharpness vs. structural sharpness**
* **energy-filtered imaging (EFI)**
  - **elemental mapping to determine local chemical composition**
* **electron holography**
  - **two-dimensional imaging *and* quantification of nanoscale electric fields**